JCB Journal of Cell Biology

ARTICLE

VASP regulates leukocyte infiltration, polarization, and vascular repair after ischemia

Hebatullah Laban[1,2], Andreas Weigert[3], Joana Zink[1,2], Amro Elgheznawy[1,2], Christoph Schürmann[2,4], Lea Günther[1,2], Randa Abdel Malik[1,2], Sabrina Bothur[5], Susanne Wingert[5], Rolf Bremer[6], Michael A. Rieger[5], Bernhard Brüne[3], Ralf P. Brandes[2,4], Ingrid Fleming[1,2], and Peter M. Benz[1,2]

In ischemic vascular diseases, leukocyte recruitment and polarization are crucial for revascularization and tissue repair. We investigated the role of vasodilator-stimulated phosphoprotein (VASP) in vascular repair. After hindlimb ischemia induction, blood flow recovery, angiogenesis, arteriogenesis, and leukocyte infiltration into ischemic muscles in VASP$^{-/-}$ mice were accelerated. VASP deficiency also elevated the polarization of the macrophages through increased signal transducer and activator of transcription (STAT) signaling, which augmented the release of chemokines, cytokines, and growth factors to promote leukocyte recruitment and vascular repair. Importantly, VASP deletion in bone marrow–derived cells was sufficient to mimic the increased blood flow recovery of global VASP$^{-/-}$ mice. In chemotaxis experiments, VASP$^{-/-}$ neutrophils/monocytes were significantly more responsive to M1-related chemokines than wild-type controls. Mechanistically, VASP formed complexes with the chemokine receptor CCR2 and β-arrestin-2, and CCR2 receptor internalization was significantly reduced in VASP$^{-/-}$ leukocytes. Our data indicate that VASP is a major regulator of leukocyte recruitment and polarization in postischemic revascularization and support a novel role of VASP in chemokine receptor trafficking.

Introduction

Ischemic vascular diseases remain a major treatment challenge (Limbourg et al., 2009). After vessel occlusion, two different responses contribute to vascular repair and tissue regeneration: angiogenesis and arteriogenesis. Angiogenesis (capillary sprouting from preexisting vasculature) is mainly initiated by hypoxia-driven VEGF release in the ischemic tissue distal to the occlusion. Arteriogenesis (enlargement/remodeling of preexisting collateral arteries into conductance vessels), on the other hand, is mainly driven by an increase of blood flow and hemodynamic changes in the collaterals proximal to and around the occlusion (Shireman, 2007; Limbourg et al., 2009). Vascular regeneration after ischemia requires complex interactions between endothelial cells, smooth muscle cells, and leukocytes. The attraction of leukocytes to the injured and hypoxic tissue by chemokines and adhesion molecules, expressed by the ischemic vasculature, plays an important role in arteriogenesis, angiogenesis, and tissue regeneration (Shireman, 2007; Griffith et al., 2014). Indeed, hindlimb ischemia studies in mice with deficient leukocyte recruitment revealed impaired angiogenesis, arteriogenesis, and restoration of blood perfusion (Scholz et al., 2000; Heil et al., 2004; Shireman, 2007). Once in the extravascular space, leukocytes themselves release a range of chemokines to initiate a positive feedback loop of leukocyte recruitment (Griffith et al., 2014). In addition to recruitment, macrophage polarization is also important for postischemic vascular remodeling. The term polarization refers to the functional skewing of the macrophage phenotype from a nonactivated state to a multitude of activated phenotypes. A classically activated or proinflammatory (M1) phenotype that occurs initially during inflammation can be reproduced in vitro using Toll-like receptor (TLR) ligands, including pathogen-associated molecular patterns such as LPS, and IFNγ. However, TLR signaling can also be activated in the absence of microbes by damage-associated molecular patterns and endogenous ligands, which are released during tissue injury and matrix degradation (Anders and Schaefer, 2014). Skewing of macrophage function toward the M1 phenotype via STAT1 is characterized by high expression levels of inducible nitric oxide synthase (iNOS), TNF-α, IL-1β, VEGF, CD80, and other proteins (Sica and Mantovani, 2012). Later in the inflammation process, macrophage gene expression changes and the expression of

[1]Institute for Vascular Signalling, Centre for Molecular Medicine, Goethe University, Frankfurt am Main, Germany; [2]German Centre of Cardiovascular Research (DZHK), Partner site Rhein-Main, Frankfurt am Main, Germany; [3]Institute of Biochemistry I-Pathobiochemistry, Faculty of Medicine, Goethe University, Frankfurt am Main, Germany; [4]Institute for Cardiovascular Physiology, Goethe University, Frankfurt am Main, Germany; [5]LOEWE Center for Cell and Gene Therapy and Department for Medicine, Hematology/Oncology, Goethe University, Frankfurt am Main, Germany; [6]HBB Datenkommunikation and Abrechnungssysteme, Hannover, Germany.

Correspondence to Peter M. Benz: benz@vrc.uni-frankfurt.de.

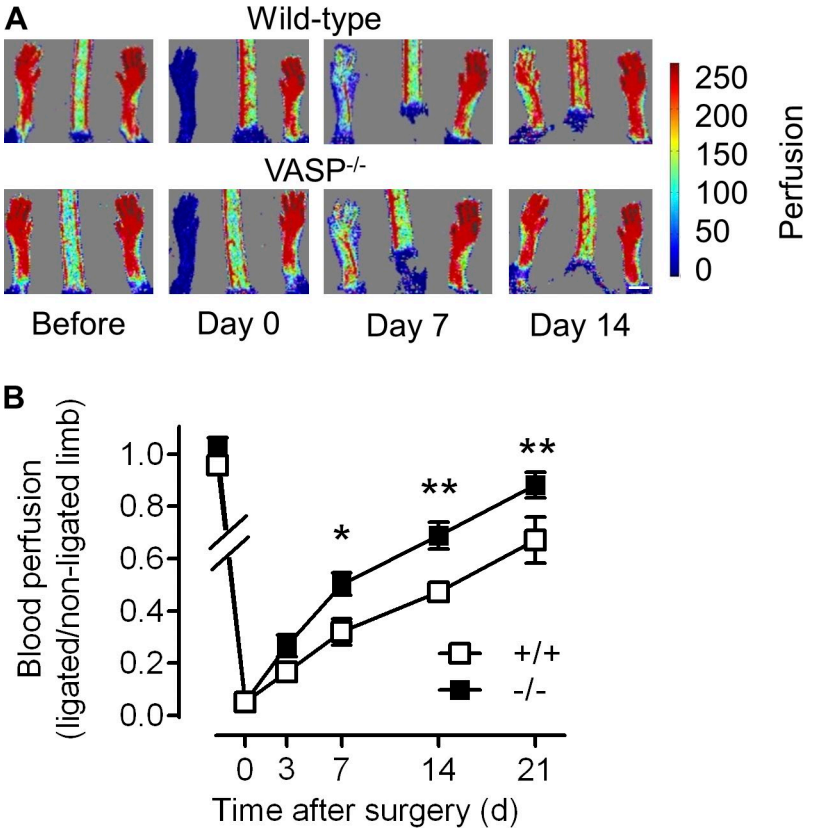

Figure 1. **Improved blood flow recovery in VASP$^{-/-}$ mice after ischemia.** WT (+/+) and VASP$^{-/-}$ (−/−) mice underwent femoral artery excision, and blood flow recovery was assessed by laser Doppler imaging immediately before (day −1) and after ligation (days 0, 3, 7, 14, and 21). Bar, 5 mm. **(A)** Representative laser Doppler images. **(B)** Time course of the recovery of blood flow as the ratio of the ligated to nonligated hindlimb; n = 10 animals per group; error bars, SEM; *, P < 0.05; **, P < 0.01 (two-way ANOVA/Bonferroni).

proteins attributed to wound-healing actions increases, a phenomenon that goes hand-in-hand with the resolution of inflammation. This macrophage subtype is referred to as alternatively activated or wound-healing (M2) macrophage and can be simulated in vitro using IL-4 (Sica and Mantovani, 2012; Tugal et al., 2013). Skewing macrophage function toward the M2 phenotype via STAT6 is characterized by high expression levels of IL-10, arginase 1, Ym1, resistin-like molecule-α (Fizz1), and CD206, among others. Considering the broad spectrum of macrophage plasticity in vivo, the M1/M2 classification of macrophages is now considered an oversimplified approach. However, with regard to ischemic vascular diseases, previous studies have indicated a role of M1-like macrophages in initiation of angiogenesis, whereas M2-like macrophages promote vessel maturation and support arteriogenesis (Fung and Helisch, 2012; Spiller et al., 2014).

The extravasation of monocytes into inflamed tissue is a well-orchestrated process that depends on transvascular chemokine gradients and adhesion molecule expression as well as leukocyte actin dynamics (Perri et al., 2007; Griffith et al., 2014). Vasodilator-stimulated phosphoprotein (VASP) is an important mediator of actin dynamics and migration of several cell types including fibroblasts and cancer cells (Krause and Gautreau, 2014). In macrophages, VASP is required for efficient phagocytosis (Coppolino et al., 2001), and Ena, a *Drosophila* homologue of VASP, regulates invasive migration of macrophage-like hemocytes in vivo (Tucker et al., 2011). Recently, the nitric oxide–VASP signaling cascade was shown to participate in activation of Kupffer cells (liver macrophages) and hepatic inflammation (Lee et al., 2015). However, whether or not VASP is required for postischemic vascular remodeling is currently unknown. The aim of the present study was to assess the role of VASP in the regulation of vascular repair in the mouse hindlimb ischemia model and determine the mechanisms involved.

Results

Improved vascular repair in VASP$^{-/-}$ mice after ischemia

To study the role of VASP in vascular repair, we compared vascular regeneration after ischemia in WT and VASP$^{-/-}$ mice. Laser Doppler imaging revealed that the recovery of hindlimb perfusion after femoral artery excision was accelerated in VASP$^{-/-}$ mice compared with their WT littermates (Fig. 1). A trend toward improved perfusion was already evident 3 d after surgery, reached significance at 7 d, and remained elevated until the end of the observation period (21 d).

Because laser Doppler measurements are restricted to the superficial skin blood flow, micro–computed tomography (µCT) studies were performed to assess arteriogenesis in the thigh muscles of WT mice and VASP$^{-/-}$ littermates. In ischemic hindlimbs from WT mice, 21 d after the induction of ischemia, collaterals were clearly remodeled and developed their typical "corkscrew" morphology (Limbourg et al., 2009). The magnitude of arteriogenesis, however, was much more pronounced in thigh muscles from VASP$^{-/-}$ mice (Fig. 2 A and Videos 1 and 2). The increased number and diameter of collaterals in the VASP$^{-/-}$ mice was also evident in transverse µCT sections (Fig. 2 B) and reflected in an increase in blood vessel volume in the ligated limbs (Fig. 2 C). Importantly, blood vessel volumes in the nonligated, contralateral

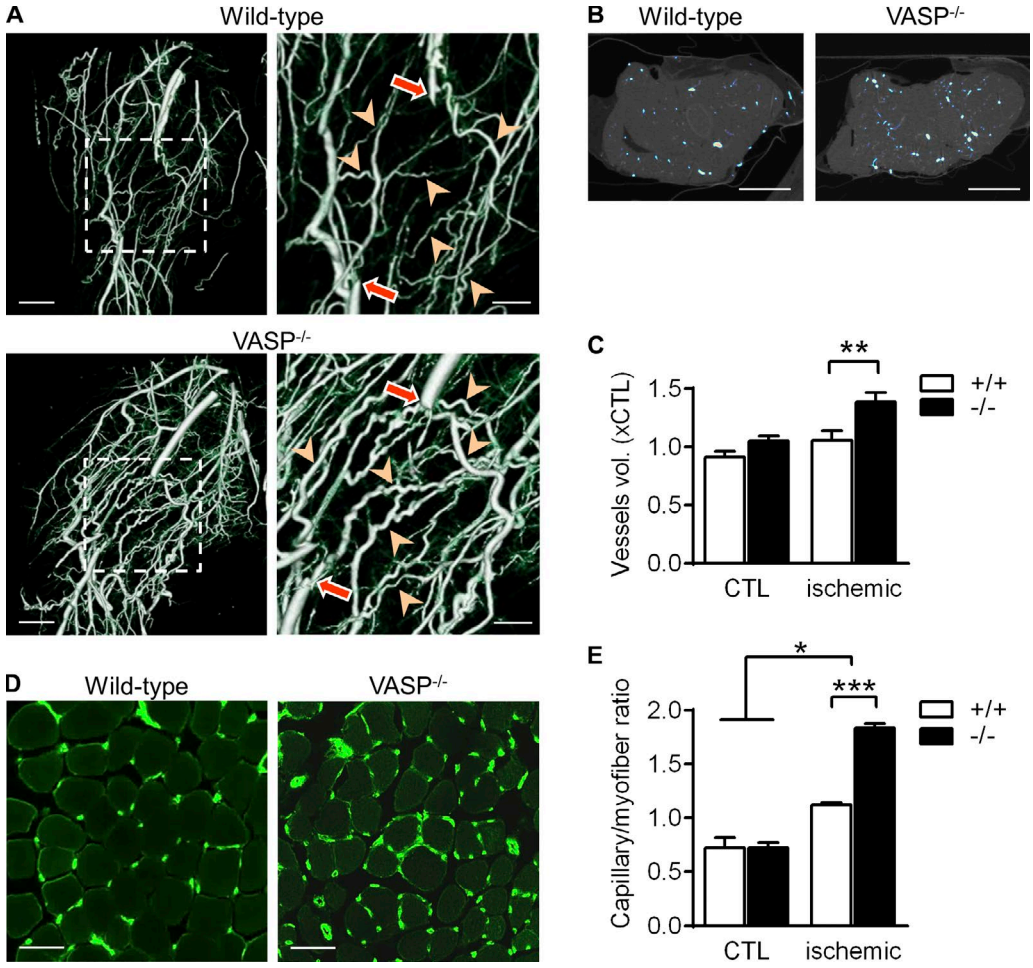

Figure 2. **Increased arteriogenesis and angiogenesis in VASP$^{-/-}$ mice after ischemia. (A)** µCT images of collateral vessel formation in the thigh muscle of WT (+/+) and VASP$^{-/-}$ (−/−) mice. In the righthand panels, arrows indicate the excision sites and arrowheads highlight the remodeled collaterals. Bars: (left panels) 2.5 mm; (magnified views) 1.25 mm. **(B)** Density of collateral vessels in the transverse section of the thigh muscle. Bars, 2.5 mm. **(C)** Total blood vessel volumes quantified from the µCT images of the ischemic and nonischemic control limb (CTL); *n* = 5 different animals per group. **(D)** Immunohistochemistry showing the capillarization (CD31, green) of the calf muscle 7 d after ischemia induction. Bars, 50 µm. **(E)** Capillary densities quantified from the immunohistochemistry images of the ischemic and nonischemic (CTL) calf muscles 7 d after ischemia induction; *n* = 5 different animals per group. Error bars, SEM; *, P < 0.05; **, P < 0.01; ***, P < 0.001 (two-way ANOVA/Bonferroni).

limbs of WT and VASP$^{-/-}$ mice were not different. Consistent with the blood flow and µCT data, capillary density (taken as angiogenesis index) in ischemic calf muscles was significantly higher in VASP$^{-/-}$ than WT mice 7 d after surgery (Fig. 2 D). Capillary densities in the nonligated limbs of WT and VASP$^{-/-}$ mice were again not different, indicating that the increased angiogenesis in VASP$^{-/-}$ mice is hypoxia dependent (Fig. 2 E).

Increased leukocyte infiltration in VASP$^{-/-}$ mice after ischemia

When we analyzed the ischemic thigh muscles from WT and VASP$^{-/-}$ mice in more detail, we observed the accumulation of leukocytes around collateral vessels in both groups. However, leukocyte numbers were significantly greater in samples from VASP$^{-/-}$ mice (Fig. 3 A). More detailed analysis of leukocyte infiltration by FACS (Fig. S1, A and B) revealed that VASP deficiency altered both the kinetics and magnitude of leukocyte infiltration. Although neutrophil numbers in ischemic thigh muscles from WT mice were elevated 3 d after ligation but returned to almost preischemic levels by day 7, neutrophil numbers remained elevated in muscles from VASP$^{-/-}$ mice (Fig. 3 B). A similar trend was observed for infiltrating monocytes (Fig. 3 C). Using CD80 and CD206 to identify proinflammatory (M1-related) versus alternatively activated (M2-related) macrophages, it was evident that VASP deletion predominantly affected classically activated macrophages in the thigh muscle (Fig. 3, D and E).

Leukocyte numbers were also increased in the calf muscles from VASP$^{-/-}$ mice (Fig. 3, F–J); however, there were two major differences. First, the overall number of infiltrated CD11b^{+} leukocytes per gram of ischemic tissue was approximately twofold higher than in the thigh muscle. However, neutrophil and monocyte numbers had already returned to baseline 7 d after surgery irrespective of the genotype, indicating that the hypoxia in the calf muscle is a stronger but more transient trigger for leukocyte recruitment (Fig. 3, G and H). Second, numbers of M2 polarized macrophages were significantly greater in ischemic muscles from VASP$^{-/-}$ mice 7 d after surgery, potentially supporting capillary maturation (Fig. 3, I and J).

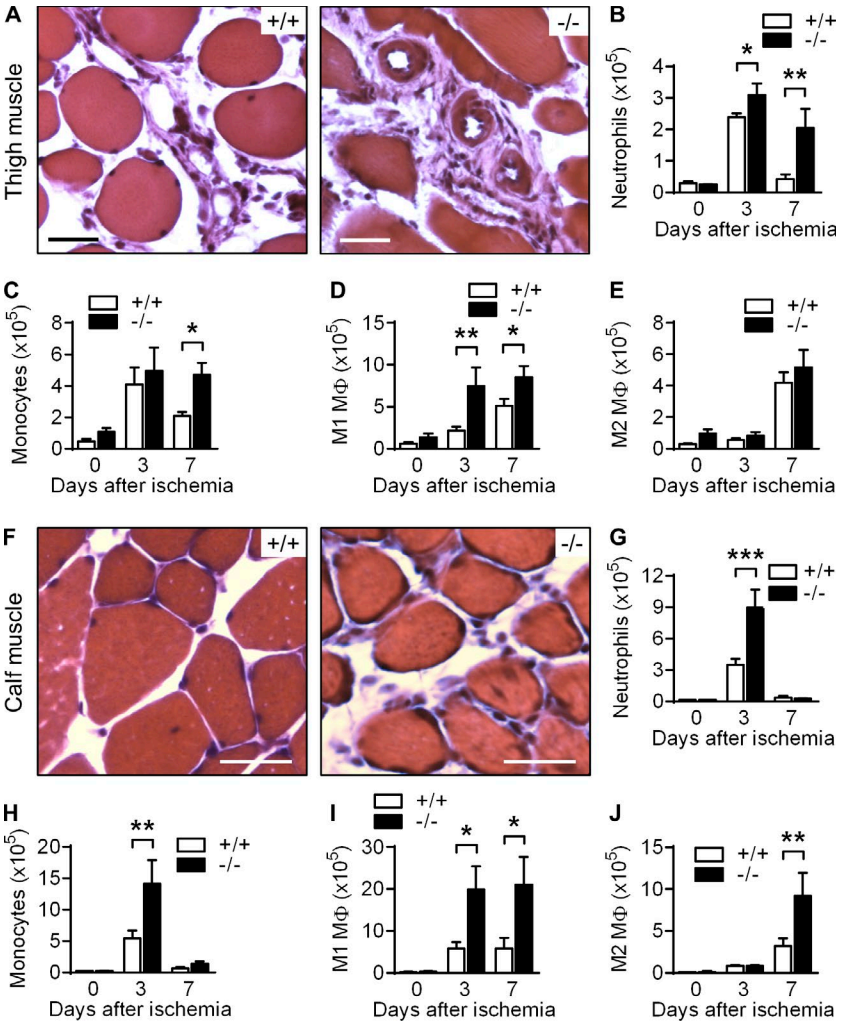

Figure 3. **Increased leukocyte infiltration in ischemic muscles of VASP$^{-/-}$ mice.** Hematoxylin and eosin–stained sections of ischemic thigh (A) and calf (F) muscles from WT (+/+) and VASP$^{-/-}$ (−/−) mice, 7 d after induction of ischemia. Bars, 50 µm. Bar graphs show the quantification of leukocyte numbers isolated from thigh (B–E) and calf (G–J) muscles per gram of tissue before ischemia induction (0) and 3 or 7 d after ischemia induction: neutrophils (B and G), monocytes (C and H), M1-related macrophages (D and I), and M2-related macrophages (E and J). n = 6 animals per group; error bars, SEM; *, P < 0.05; **, P < 0.01; ***, P < 0.001 (two-way ANOVA/Bonferroni).

VASP expression in mouse leukocytes

To obtain first insight into a potential role of VASP in leukocyte transmigration, we isolated bone marrow (BM)-derived leukocytes by FACS (Fig. S1 C) and detected VASP protein expression in monocytes and neutrophils from WT but not from VASP$^{-/-}$ mice (Fig. 4 A). VASP expression was maintained after the differentiation of monocytes to macrophages. Although incubation with LPS and IFNγ increased VASP expression by almost threefold, alternative macrophage activation induced by IL-4 significantly decreased VASP mRNA levels (Fig. 4 B). The M1-related increase in VASP mRNA was biphasic, peaking at 6 h after stimulation but remaining elevated over control levels for up to 60 h (Fig. 4 C). The increase in VASP mRNA expression in M1 polarized macrophages was reflected in increased protein expression as well as VASP phosphorylation on Ser157 (Fig. 4 D). The latter observation is consistent with the M1-associated increase in iNOS expression, which leads to the protein kinase G–mediated phosphorylation of the protein and the associated mobility shift in SDS-PAGE (Benz et al., 2009).

We also analyzed VASP expression in infiltrated leukocytes, 3 d after femoral artery excision. Similar to the sorted BM cells, FACS analyses revealed distinct VASP protein levels in neutrophils and monocytes from WT but not VASP$^{-/-}$ mice (Fig. 4 E). VASP expression was also maintained in infiltrated macrophages and appeared more robust in M1-like macrophages (Fig. 4 F).

Increased leukocyte polarization in VASP$^{-/-}$ mice after ischemia

Owing to the expression of VASP in monocytes/macrophages, we next investigated the impact of VASP on leukocyte polarization in vivo. 3 d after ischemia, proinflammatory genes, including TNF-α and IL-1β were significantly increased in leukocytes from thigh and the calf muscles of VASP$^{-/-}$ mice, whereas iNOS expression was elevated only in the hypoxic calf muscles (Fig. 5 A). Surprisingly, several anti-inflammatory genes were also up-regulated in VASP$^{-/-}$ leukocytes, including Ym1 in the thigh muscle, arginase 1 in the calf muscle, and a trend toward IL-10 in both muscles (Fig. 5 B). The hypoxia-inducible factors HIF-1α and HIF-2α play a role in regulating macrophage polarization, with HIF-1α controlling iNOS and VEGF expression and the M1-related state, and HIF-2α regulating arginase 1 expression and the M2-related phenotype (Takeda et al., 2010). Consistent with increased iNOS, arginase 1 and VEGF levels in the hypoxic calf muscles, HIF-1α and HIF-2α levels were significantly up-regulated in leukocytes from this tissue (Fig. 5 C). However, only HIF-2α was elevated in VASP$^{-/-}$ leukocytes from the thigh muscle, likely reflecting the

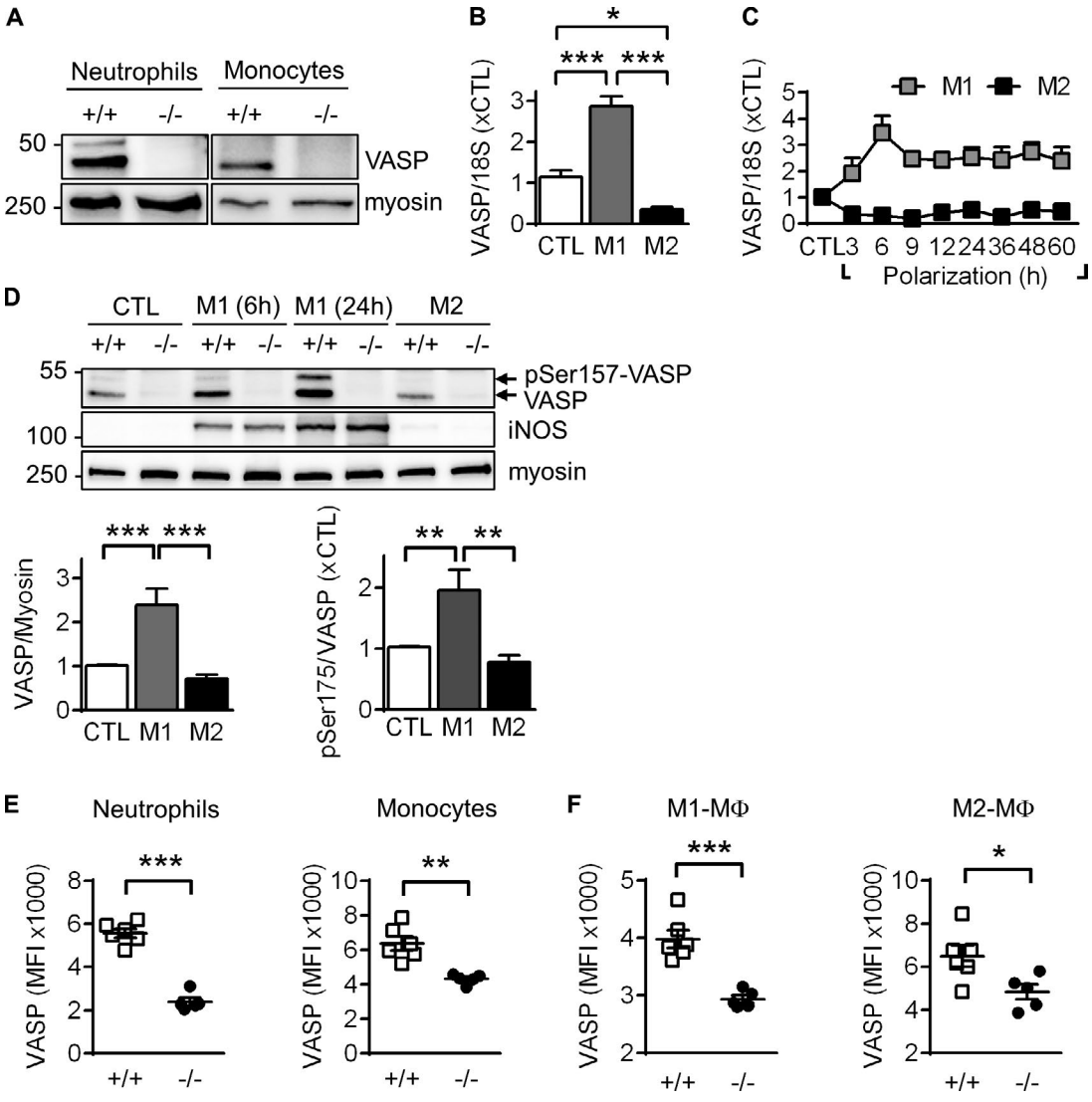

Figure 4. **VASP expression in mouse leukocytes and polarized macrophages. (A)** Western blots of VASP expression in BM-derived neutrophils and monocytes isolated by FACS from WT (+/+) and VASP$^{-/-}$ (−/−) mice. Myosin served as loading control. One representative experiment of a series of four is shown. **(B)** VASP mRNA levels in mouse BM–derived CTL macrophages, as well as after M1 (10 ng/ml LPS and 1 ng/ml IFNγ, 24 h) or M2 (25 ng/ml IL-4, 24 h) stimulation; *n* = 9 animals per group. **(C)** Time course of changes in VASP mRNA levels after M1 or M2 polarization; *n* = 4 animals per group. **(D)** Effect of macrophage polarization (6 or 24 h) on VASP protein levels and phosphorylation. iNOS expression is shown as a control for M1 polarization. **(E and F)** FACS analysis of VASP protein levels in leukocytes infiltrated into the hindlimb 3 d after femoral artery excision. *n* = 5–8 animals per group; error bars, SEM; *, P < 0.05; **, P < 0.01; ***, P < 0.001 (Student's *t* test).

more pronounced hypoxia in the calf muscle. Given that VASP deficiency affects leukocyte populations in the ischemic hindlimb, we verified the role of VASP in macrophage polarization in vitro. Very similar to the in vivo situation, VASP deletion significantly increased the mRNA levels of pro- and anti-inflammatory genes in pure M1 and M2 macrophage populations, respectively (Fig. S2, A–I). Next, we quantified the protein levels of TNFα in the ischemic calf muscle and iNOS in in vitro polarized macrophages. Consistent with the mRNA levels, VASP deletion significantly increased both proteins (Fig. S2, J and K).

Increased STAT signaling in VASP$^{-/-}$ macrophages in vitro

STAT1 and STAT6 are activated downstream of IFNγ/TLR4 or IL-4 signaling to skew macrophage function toward the M1- or M2-related phenotype, respectively (Sica and Mantovani, 2012). Consistent with the increased levels of proinflammatory genes, such as TNFα and iNOS, in VASP$^{-/-}$ M1 macrophages in vitro (Fig. S2, A–F), STAT1 expression was significantly up-regulated in these leukocytes compared with WT controls (Fig. 6 A). Preincubation with the STAT1 inhibitor fludarabine (Frank et al., 1999) completely blunted the increased expression of TNFα and iNOS in VASP$^{-/-}$ M1 macrophages and expression levels of the genes were indistinguishable between WT and VASP$^{-/-}$ cells (Fig. 6, B and C). This indicates that elevated STAT1 signaling is likely the cause for the increased M1 polarization of VASP$^{-/-}$ macrophages.

Consistent with the increased arginase and Fizz1 levels in VASP$^{-/-}$ M2 macrophages in vitro (Fig. S2, G and H), STAT6 phosphorylation was significantly increased in these leukocytes compared with WT controls (Fig. 6 D). However, preincubation with the specific STAT6 inhibitor AS1517499 (Chiba et al., 2009)

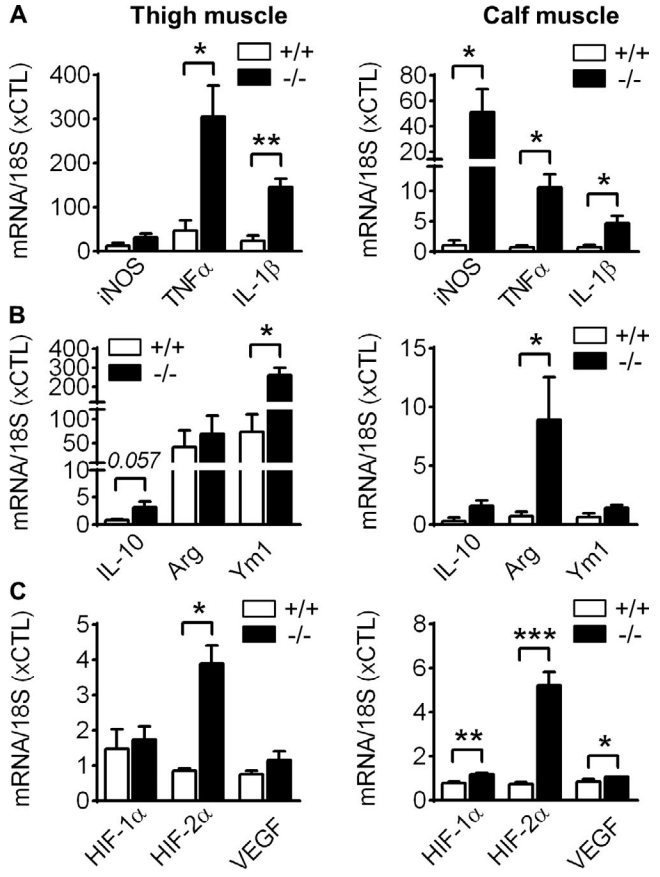

Figure 5. **Increased polarization of VASP$^{-/-}$ leukocytes in vivo.** qPCR analysis of infiltrated leukocytes, isolated from the ischemic thigh and calf muscles from WT (+/+) and VASP$^{-/-}$ (−/−) mice 3 d after femoral artery excision. **(A)** Expression of the proinflammatory genes iNOS, TNF-α, and IL-1β. **(B)** Expression of the anti-inflammatory genes IL-10, arginase 1, and Ym1. **(C)** Expression of the hypoxia-related genes HIF1α, HIF2α, and VEGF. *n* = 5 animals per group, error bars, SEM; *, P < 0.05; **, P < 0.01; ***, P < 0.001 (Student's *t* test).

fully blocked the increased expression of the anti-inflammatory macrophage marker genes, suggesting that increased STAT6 signaling is (at least partially) the reason underlying the increased M2 polarization in VASP$^{-/-}$ macrophages (Fig. 6, E and F).

VASP$^{-/-}$ BM–derived cells improve blood flow recovery after ischemia

Vascular regeneration after ischemia requires complex interactions between endothelial cells, smooth muscle cells, and leukocytes. Therefore, we determined whether VASP deficiency specifically within the BM lineage (including neutrophils and monocytes/macrophages) is sufficient to increase vascular repair after ischemia. WT or VASP$^{-/-}$ BM was transplanted into sublethally irradiated WT and VASP$^{-/-}$ mice. After a recovery period of 10 wk, transplanted animals underwent hindlimb ischemia, and successful engraftment was confirmed by genotyping of blood-derived leukocytes (Fig. 7 A). Similar to global VASP$^{-/-}$ mice (Fig. 1), VASP$^{-/-}$ mice transplanted with VASP$^{-/-}$ BM displayed a significantly improved blood flow recovery compared with WT mice transplanted with WT BM (Fig. 7 B). More importantly, reconstitution of WT mice with VASP$^{-/-}$ BM significantly accelerated the recovery of hindlimb perfusion, albeit a significant difference was observed only starting at day 14 after surgery (Fig. 7 C). Conversely, reconstitution of VASP$^{-/-}$ mice with WT BM significantly delayed blood flow recovery (Fig. 7 D). Notably, there was no difference in blood perfusion between WT and VASP$^{-/-}$ mice that both received WT BM (Fig. 7 E). As summarized in Fig. 7 F, our data demonstrate that the deletion of VASP in BM-derived cells is sufficient to mimic the phenotype seen in the global VASP$^{-/-}$ mice.

Impact of VASP deletion on chemokine release and leukocyte responsiveness

In vivo, macrophage activation leads to production of a wide range of chemokines including CXCL1 and CCL2, which initiate the recruitment and transendothelial migration of neutrophils and monocytes into the inflamed tissue via CXCR2 and CCR2 chemokine receptors, respectively (Shireman, 2007; Souto et al., 2011; Griffith et al., 2014). Given that leukocyte numbers were increased in ischemic muscles of VASP$^{-/-}$ mice, we analyzed whether VASP deficiency affects chemokine release by macrophages and/or leukocyte responsiveness during chemotaxis.

We studied chemokine release in ischemic calf muscles 3 d after femoral artery excision, because changes in leukocyte recruitment between WT and VASP$^{-/-}$ mice were most pronounced at this point in time. Protein and mRNA levels of CXCL1 and CCL2 were both significantly up-regulated in ischemic muscles from VASP$^{-/-}$ mice (Fig. 8, A and B; and Fig. S3 A). Importantly, CXCL1 and CCL2 mRNA levels were also significantly increased in VASP$^{-/-}$ M1 macrophages in vitro (Fig. 8, C and D), indicating that elevated chemokine levels in the ischemic muscles of VASP$^{-/-}$ mice were at least partially caused by the increased activation of VASP$^{-/-}$ macrophages.

Next, the impact of VASP deletion on leukocyte responsiveness (chemotaxis) through Transwell filters was assessed in vitro, and migrated leukocytes were identified by FACS (Fig. S1 D). To mimic the in vivo situation, we used conditioned medium from WT nonpolarized (control) or M1 or M2 macrophages as chemoattractant. Only few neutrophils/monocytes migrated in response to the conditioned medium from nonpolarized macrophages, and there was no difference between WT and VASP$^{-/-}$ leukocyte chemotaxis (Fig. 8, E and F). Conditioned medium from M1 macrophages increased the number of migrating neutrophils (Fig. 8 E) and monocytes (Fig. 8 F) in both groups, with migration capacity being significantly greater in cells from VASP$^{-/-}$ mice, especially in monocytes. Similar results were obtained when CCL2 (the classic ligand of CCR2) was used as chemoattractant (Fig. S3 B). M2 conditioned medium had no impact on neutrophil chemotaxis but markedly elevated the number of migrated monocytes. There was no difference, however, in the migration of WT and VASP$^{-/-}$ monocytes. Together, these findings indicate that VASP deficiency specifically modifies leukocyte chemotaxis in response to M1-related chemokines.

Given their role in leukocyte migration and infiltration, we next compared the surface expression of CXCR2 and CCR2 chemokine receptors in WT and VASP$^{-/-}$ cells. Under basal conditions, there was no difference in CXCR2 or CCR2 surface expression in neutrophils and monocytes from WT and

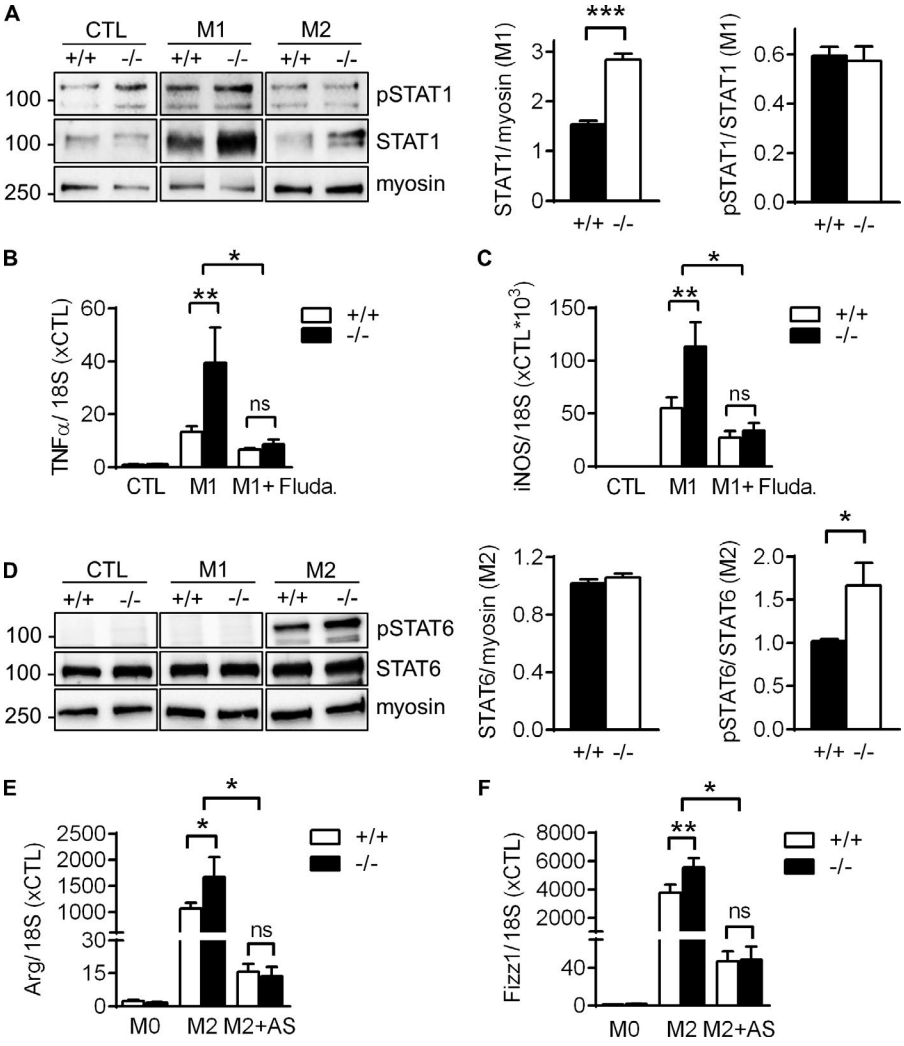

Figure 6. **Increased STAT signaling in VASP$^{-/-}$ macrophages in vitro. (A)** Western blot analyses of STAT1 expression and phosphorylation (pSTAT1) in macrophages from WT and VASP$^{-/-}$ mice without (CTL) or with in vitro polarization to M1 with LPS (10 ng/ml) and IFNγ (1 ng/ml) for 24 h or to M2 with IL-4 (25 ng/ml) for 24 h. (n = 5, Student's t test). **(B and C)** qPCR analysis of the proinflammatory genes TNFα (B) and iNOS (C) in mouse BM–derived CTL macrophages, M1 macrophages, or macrophages that were preincubated with the STAT1 inhibitor fludarabine (Fluda, 50 µM) for 1 h before induction of M1 polarization. n = 6 (two-way ANOVA/Bonferroni). **(D)** Western blot analyses of STAT6 expression and phosphorylation (pSTAT6) in CTL, M1, or M2 macrophages from WT and VASP$^{-/-}$ mice. n = 7 (Student's t test). **(E and F)** qPCR analysis of the anti-inflammatory genes Arg (E) and Fizz1 (F) in mouse BM-derived CTL macrophages, M2 macrophages, or macrophages that were preincubated with the STAT6 inhibitor AS1517499 (AS, 2 µM) for 1 h before induction of M2 polarization. n = 8 (two-way ANOVA/Bonferroni); error bars, SEM; *, P < 0.05; **, P < 0.01; ***, P < 0.001; ns, nonsignificant.

VASP$^{-/-}$ mice (Fig. S3, C–F), and stimulation with conditioned medium from control or M2 macrophages did not significantly change the surface levels of the chemokine receptors (Fig. S3, G and H). Stimulation with M1 conditioned medium, however, which contains high levels of the CXCR2 ligand CXCL1 (Fig. S3 I), rapidly decreased CXCR2 surface expression in neutrophils (Fig. 8 G), whereas changes in CXCR2 levels in monocytes after stimulation were comparatively small (Fig. 8 H). We did not observe significant changes in CXCR2 surface expression between WT and VASP$^{-/-}$ leukocytes under these conditions (Fig. 8, G and H).

Stimulation with M1 conditioned medium, which contains high levels of the primary CCR2 ligand CCL2 (Fig. S3 J), continuously decreased CCR2 surface expression in leukocytes from WT mice (Fig. 8, I and J), which likely reflects the desensitization and internalization of the receptor. In VASP$^{-/-}$ monocytes, however, the decrease in CCR2 surface expression was significantly delayed and was even preceded by an increase in CCR2 surface expression in VASP$^{-/-}$ neutrophils (Fig. 8, I and J).

Together, our data indicate that VASP deficiency elevates both the chemokine release by macrophages and the responsiveness of circulating leukocytes, and thereby synergistically increases leukocyte recruitment into the inflamed tissue.

Impact of Rac1 activity and actin dynamics on CCR2 surface levels

Next, we aimed to determine how VASP may be implicated in CCR2 receptor internalization. Previously, VASP has been shown to modulate the activity of the small GTPase Rac1 in a cell type– and context-dependent manner (Schlegel and Waschke, 2009; Jennissen et al., 2012). Little is known about a role of Rac1 in CCR2 receptor internalization, but chemokine-induced Rac1 activation promotes lamellipodia protrusions and directed cell migration (Maghazachi, 2000). Consistently, Rac1 inhibition blocked CCL2-induced monocyte chemotaxis in our Transwell experiments (Fig. S4 A). However, neither activation nor inhibition of Rac1 had a significant impact on CCR2 surface levels in the same cells (Fig. S4 B), suggesting that VASP-dependent Rac1 activation is most likely not causative for changes in CCR2 receptor trafficking in VASP$^{-/-}$ monocytes.

Actin polymerization participates in receptor-mediated endocytosis in mammalian cells, but underlying mechanisms and affected receptors are not well understood (Kaksonen et al., 2006; Mooren et al., 2012). Given that VASP is an important regulator of actin dynamics, we analyzed whether inhibition of actin dynamics affects CCR2 receptor internalization. Preincubation of monocytes with latrunculin B (5 µM) significantly changed

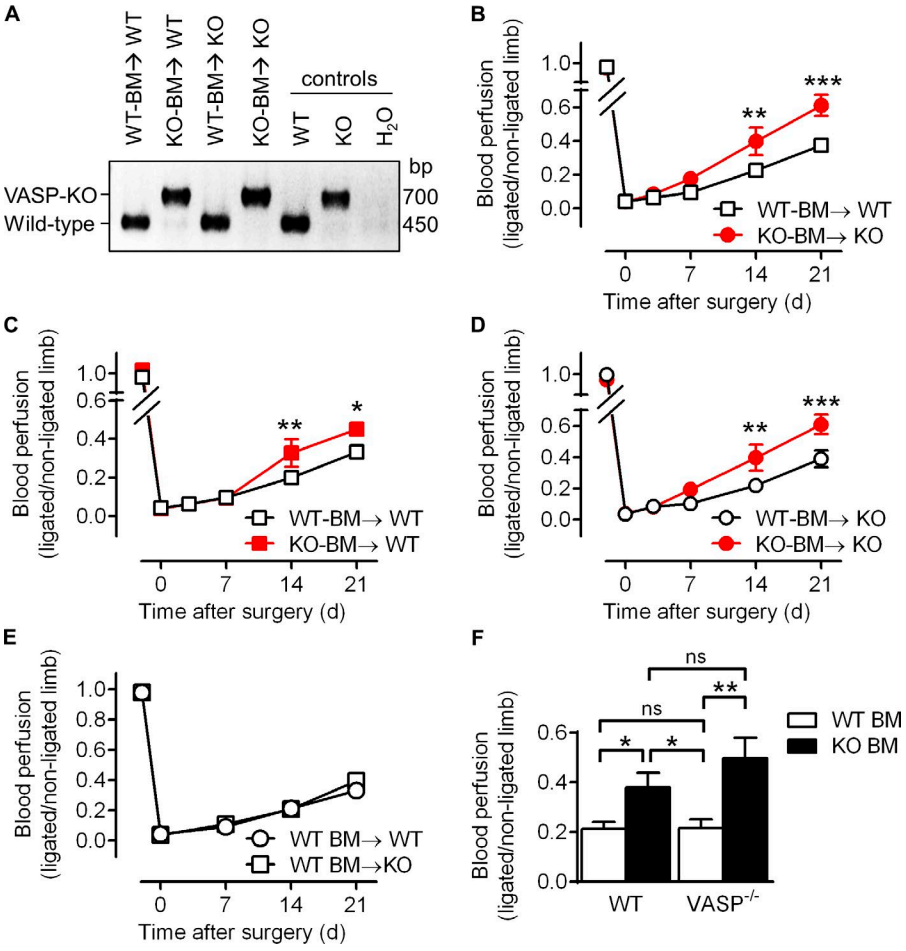

Figure 7. **VASP$^{-/-}$ BM–derived cells improve blood flow recovery after ischemia.** Four groups of BM transplanted animals, WT-BM→WT (WT BM transplanted into WT mice), WT-BM→KO (WT BM transplanted into VASP$^{-/-}$ mice), KO-BM→WT (VASP$^{-/-}$ BM transplanted into WT mice), and KO-BM→KO (VASP$^{-/-}$ BM transplanted into VASP$^{-/-}$ mice) underwent hindlimb ischemia and laser Doppler imaging to assess blood flow recovery. **(A)** Successful engraftment was confirmed by genotyping of blood-derived leukocytes. One representative genotyping PCR of a series of four is shown; VASP KO ∼700 bp and WT ∼450 bp. **(B–E)** Time course of the recovery of blood flow as the ratio of the ligated to nonligated hindlimb. Transplanted VASP$^{-/-}$ or WT BM is indicated in red and black, respectively. Recipient VASP$^{-/-}$ or WT mice are indicated by circles and squares, respectively. **(F)** Comparison of blood perfusion of all four groups 14 d after femoral artery excision. WT and VASP$^{-/-}$ transplanted BM is indicated by white and black bars, respectively. The genotype of the recipient mice is shown below the bars. n = 8–10 animals per group; error bars, SEM; *, P < 0.05; **, P < 0.01; ***, P < 0.001 (two-way ANOVA/Bonferroni).

CCR2 receptor internalization (Fig. S4, C and D). Although this pharmacologic approach supports a role of actin in CCR2 receptor trafficking, further experiments are required to address a potential role of VASP in this process.

VASP forms complexes with CCR2 and β-arrestin 2 in leukocytes

The CCR2 chemokine receptor follows the canonical G protein–coupled receptor (GPCR) trafficking pathway. After receptor activation, the cytoplasmic tail of the receptor is rapidly phosphorylated, which prevents further activation. Phosphorylated receptors interact with one of the β-arrestins, which target the receptor for internalization, leading to a permanent or transient loss of cell surface receptors caused by degradation or recycling, respectively (Bennett et al., 2011). Interestingly, we observed a physical association between VASP and CCR2 in BM-derived leukocytes from WT mice under basal conditions and after stimulation with M1-conditioned medium (Fig. 9 A). Similarly, antibodies directed against β-arrestin 2 immunoprecipitated VASP from lysates of leukocytes under basal conditions and pretreated with M1-conditioned medium (Fig. 9 B). The interaction of VASP and β-arrestin 2 was further confirmed by coimmunoprecipitation experiments in HEK293 cells (Fig. 9 C) as well as pull-down experiments with purified recombinant GST–β-arrestin 2 and VASP (Fig. 9 D), which indicated a direct interaction of the proteins in vitro. Under basal conditions, CCR2, β-arrestin 2, and VASP colocalized mainly at the plasma membrane of BM-derived leukocytes, whereas after CCL2 stimulation (to induce CCR2 receptor internalization) the three proteins colocalized in a subset of vesicle-like structures (Fig. 9, E and F). In addition to its role in receptor internalization, β-arrestin 2 is required for LPS-induced extracellular signal–regulated kinase (ERK) 1/2 activation in macrophages (Fan et al., 2007). Although β-arrestin 2 protein levels were significantly up-regulated in VASP$^{-/-}$ M1 macrophages (Fig. S5, A and B), ERK1/2 phosphorylation was significantly impaired in these cells (Fig. 9 G). Together, the data show that VASP, CCR2, and β-arrestin 2 form complexes in leukocytes and suggest that VASP deficiency impairs β-arrestin 2 signaling.

CCR2 inhibition blocks the increased leukocyte infiltration in VASP$^{-/-}$ mice after ischemia

Our results suggest that changes in CCR2 receptor internalization contribute to the increased responsiveness and infiltration of VASP$^{-/-}$ leukocytes. To test this hypothesis in vivo, we compared the leukocyte infiltration between WT and VASP$^{-/-}$ mice after hindlimb ischemia induction without or with application of the specific CCR2 inhibitor RS504393 (Kitagawa et al., 2004; Fig. 10 A). Leukocyte numbers were significantly increased in ischemic calf muscles of vehicle-treated VASP$^{-/-}$ mice versus WT controls. Strikingly, however, the increased leukocyte infiltration in VASP$^{-/-}$ mice was blunted in the presence of the CCR2

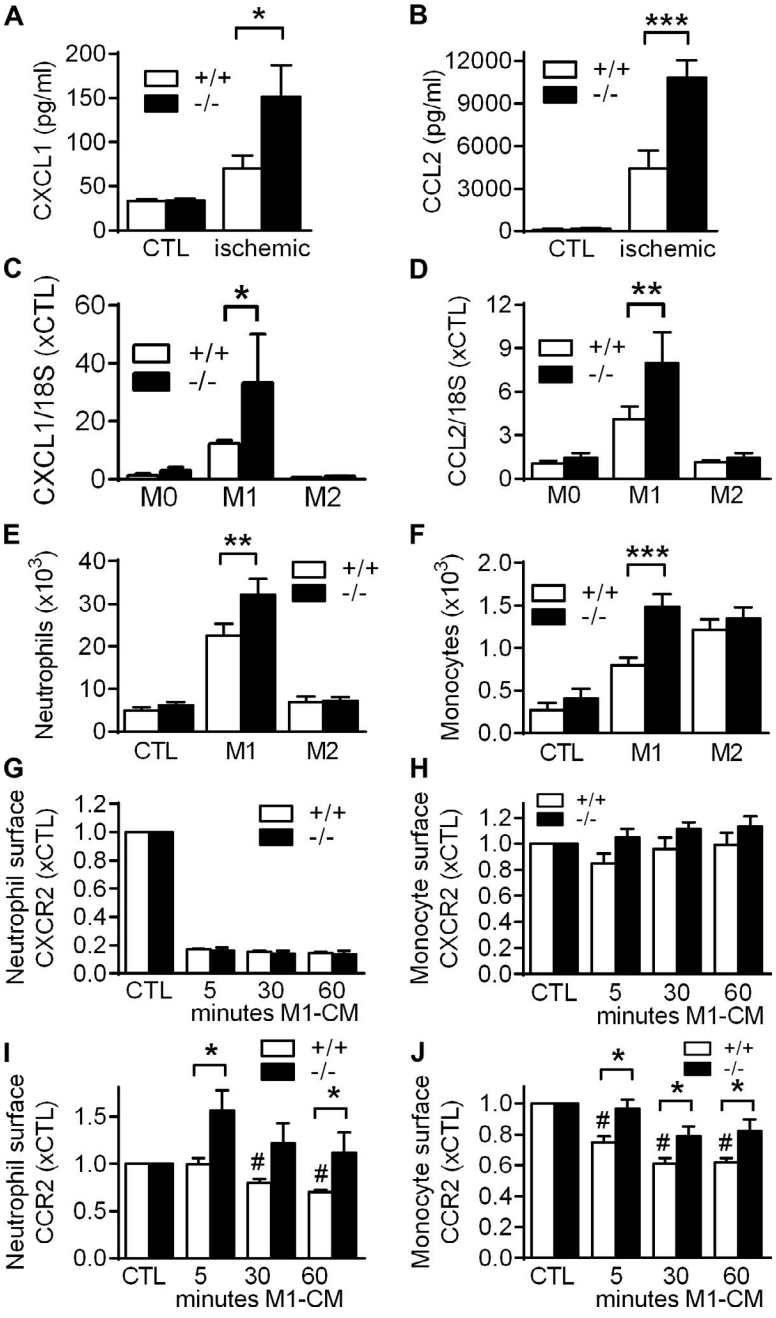

Figure 8. **Impact of VASP deletion on chemokine release and leukocyte responsiveness. (A and B)** Concentrations of CXCL1 (A) and CCL2 (B) in ischemic and CTL calf muscles of WT (+/+) and VASP$^{-/-}$ (−/−) mice 3 d after femoral artery excision (cytometric bead array); *n* = 5 mice per group. **(C and D)** CXCL1 (C) and CCL2 (D) mRNA levels in macrophages from WT (+/+) and VASP$^{-/-}$ (−/−) mice after in vitro polarization to M1 with LPS (10 ng/ml) and IFNγ (1 ng/ml) for 24 h or to M2 with IL-4 (25 ng/ml) for 24 h; *n* = 5 cell batches per group. **(E and F)** Migration of WT (+/+) and VASP$^{-/-}$ (−/−) BM–derived neutrophils (E) or monocytes (F) through Transwell filters using conditioned medium of nonpolarized (CTL), M1, or M2 macrophages as chemoattractant; *n* = 6 different cell batches per group. **(G–J)** Time course of changes in relative surface levels of the CXCR2 (G and H) and CCR2 (I and J) chemokine receptor in BM-derived neutrophils (G and I) and monocytes (H and J) after stimulation with M1 macrophage conditioned medium (M1-CM) for 5, 30, and 60 min; *n* = 5 different mice per group. Error bars, SEM; *, P < 0.05; **, P < 0.01; ***, P < 0.001; #, P < 0.01 vs. CTL$^{+/+}$ (all tests two-way ANOVA/Bonferroni).

inhibitor, and neutrophil, monocyte, and M1-like macrophage numbers were indistinguishable from WT controls (Fig. 10, B–D). This finding was further confirmed in a second, independent in vivo model, thioglycollate-induced peritonitis. Very similar to the hindlimb ischemia model, increased leukocyte infiltration into the peritoneal cavity of VASP$^{-/-}$ mice could be blocked by CCR2 inhibition (Fig. S5, C–E), supporting that the chemokine receptor CCR2 is (at least partially) responsible for the elevated leukocyte infiltration into the inflamed tissue in VASP$^{-/-}$ mice.

Discussion

The present study indicates that VASP is a major regulator of leukocyte function in vivo. In the absence of VASP, the infiltration/polarization of leukocytes was increased to contribute to accelerated angiogenesis in the calf muscle (e.g., by increased production of cytokines and growth factors, such as VEGF) and arteriogenesis in the thigh muscle, and improved after ischemic blood perfusion. The mechanisms involved seem related to changes in STAT signaling, chemokine release, and leukocyte responsiveness.

A sequential cascade of gene regulation follows the inflammatory activation of leukocytes (Wells et al., 2005). Early response genes, such as TNFα, which elicit inflammation and leukocyte recruitment, peak between 2 and 7 h after stimulation and then decline rapidly. This is followed by a second (late) wave of transcriptional activation that results in the increased expression of genes such as arginase-1 or IL-10 (Fig. S5 F). The latter can

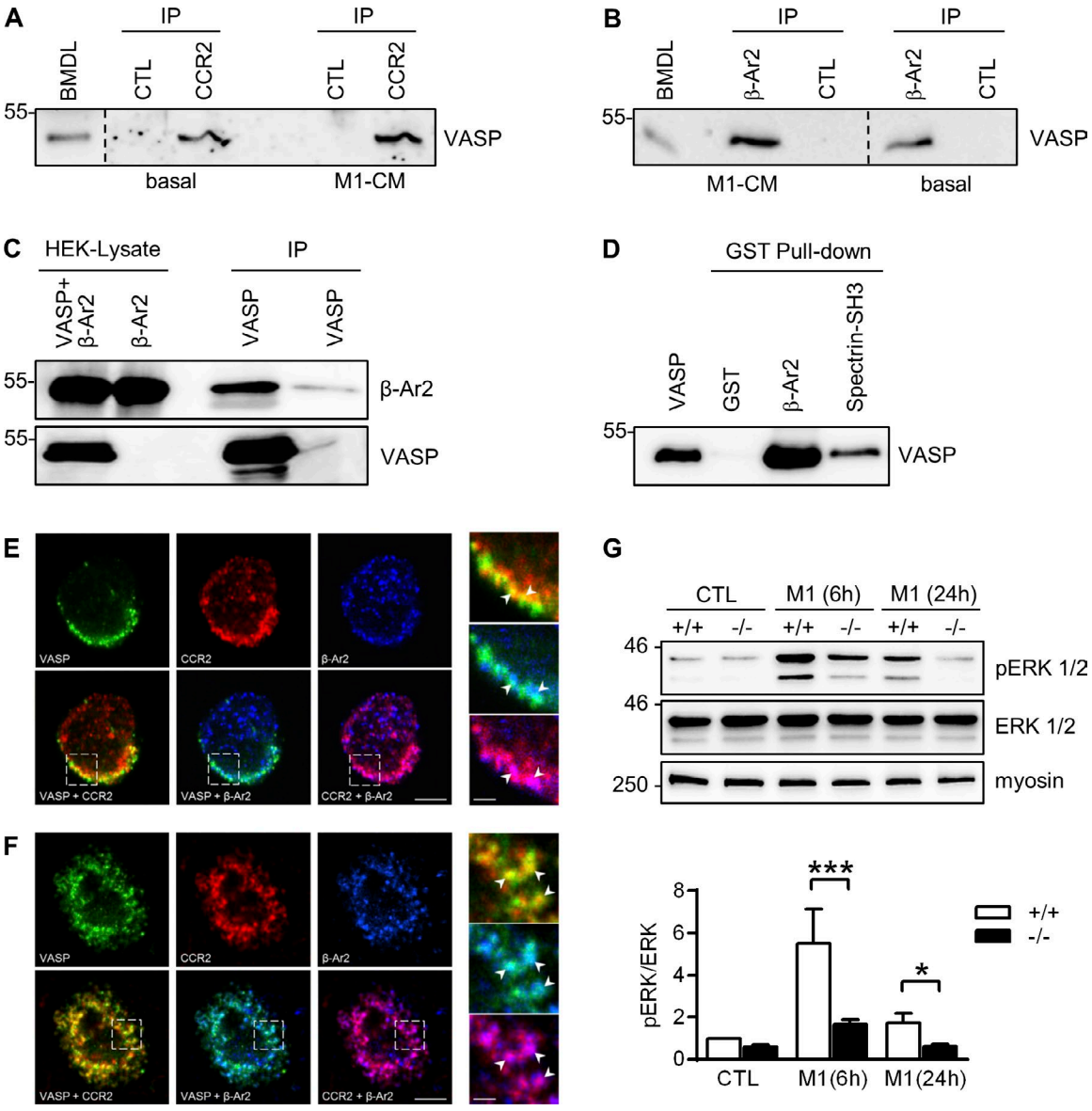

Figure 9. **VASP forms complexes with CCR2 and β-arrestin 2 in leukocytes. (A and B)** Immunoprecipitation (IP) of VASP from BM-derived leukocytes under basal conditions and after incubated with M1 conditioned medium (M1-CM) using antibodies directed against CCR2 (A) or β-arrestin 2 (β-Ar2, B). A and B show different regions of the same blot; separations are indicated. **(C)** HEK cells were transfected with β-Ar2 with or without VASP. After IP of VASP, the precipitated material was probed with β-Ar2 antibodies. **(D)** Purified recombinant VASP was pulled down with GST (negative control), GST-β-Ar2, or GST-Spectrin-SH3 (positive control), and the precipitated material was probed with VASP-specific antibodies. **(E and F)** Colocalization of VASP (green) with CCR2 (red) and β-arrestin 2 (blue) in BM-derived monocytes under basal conditions (E) and after stimulation with mouse CCL2 (150 nmol/liter; F). Bars, 4 µm. The panels on the right are higher magnifications of the areas marked by the boxes. Bars, 1 µm. Comparable results of A–E were obtained in four additional experiments. **(G)** Analysis of ERK (also termed p42/p44 MAPK) phosphorylation in WT (+/+) and VASP$^{-/-}$ (−/−) CTL macrophages and macrophages after 6 or 24 h of M1 polarization (10 ng/ml LPS and 1 ng/ml IFNγ). Myosin served as loading control. *n* = 8 animals per group; error bars, SEM; *, P < 0.05; ***, P < 0.001 (two-way ANOVA/Bonferroni).

remain elevated for at least 24 h and are considered inflammation suppressor genes because they prevent additional leukocyte recruitment and activation (Wells et al., 2005). VASP expression was rapidly but also persistently elevated in M1-activated macrophages, indicating a dual role for VASP in pro- as well as anti-inflammatory leukocyte signaling (Wells et al., 2005). Such a dual role in inflammation/resolution has been described for iNOS, which is induced by TLR ligands and IFNγ. Clearly, iNOS is important for host defense, but at the same time, myeloid iNOS expression suppresses M1 macrophage polarization (Lu et al., 2015). Increased iNOS expression in M1 macrophages correlated with VASP phosphorylation, but whether VASP phosphorylation contributes to host defense is currently unclear. Consistent with a role as an anti-inflammatory mediator, however, VASP deletion caused a pronounced inflammatory phenotype, likely induced by increased STAT1 signaling. Persistent or excessive inflammation can delay tissue repair or even exaggerate tissue damage by generation of oxidative stress (Shireman, 2007). However, anti-inflammatory genes and M2-like macrophage numbers were also increased in the ischemic tissue of VASP$^{-/-}$ mice, suggesting

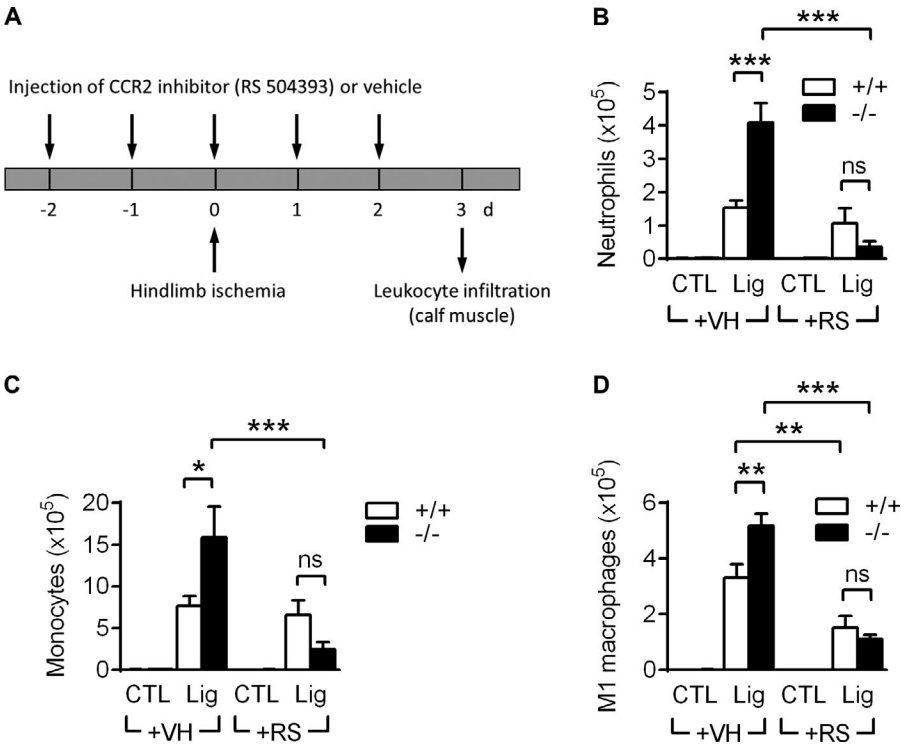

Figure 10. **CCR2 inhibition blocks the increased leukocyte infiltration in VASP$^{-/-}$ mice after hindlimb ischemia. (A)** Time protocol showing the daily injection of the CCR2 inhibitor RS504393 (+RS; 4 mg/kg per day) or vehicle (+VH) from 2 d before until 2 d after femoral artery excision. Leukocyte infiltration into ischemic and control calf muscles was analyzed by FACS 3 d after hindlimb ischemia induction. **(B–D)** Quantification of leukocyte numbers isolated from calf muscles per gram of tissue 3 d after ischemia induction: neutrophils (B), monocytes (C), and M1-related macrophages (D). $n = 6$ animals per group; error bars, SEM; *, $P < 0.05$; **, $P < 0.01$; ***, $P < 0.001$; ns = nonsignificant (two-way ANOVA/Bonferroni).

that M2 polarization, macrophage reeducation, and resolution of inflammation are not impaired in the absence of VASP. Consistent with our data, TNFα and iNOS levels were increased in Kupffer cells from VASP$^{-/-}$ animals. In contrast to our studies, however, stimulation of VASP$^{-/-}$ macrophages with IL-4 was associated with the decreased expression of Ym1, arginase, and mannose receptor (Lee et al., 2015).

In addition to leukocytes, VASP is expressed in endothelial and smooth muscle cells (Münzel et al., 2003; Benz et al., 2008a). Currently, we cannot rule out that VASP deficiency in these cells affects vascular repair after ischemia, especially at early points in time after surgery. However, VASP deletion in BM-derived cells was sufficient to mimic the increased blood flow recovery of global VASP$^{-/-}$ mice, highlighting the fundamental role of VASP in leukocytes.

VASP (or its homologue Mena) regulates the actin-based motility of various cell types (Sechi and Wehland, 2004; Trichet et al., 2008; Krause and Gautreau, 2014), but there is considerable controversy about whether VASP is a positive (Moeller et al., 2004) or negative (Bear et al., 2000) regulator of cell migration. This is not particularly surprising given that cell movement is a complex and cell type–dependent process and that VASP is involved in many actin-dependent processes (Bear and Gertler, 2009). In contrast to random cell migration, little is known about the role of VASP in chemotaxis, and most studies were conducted either in slime mold (Han et al., 2002; Lin et al., 2010) or in cell lines overexpressing chemokine receptors (Neel et al., 2009).

Monocyte trafficking from the blood to the inflamed tissue is mainly mediated by CCL2/CCR2 interactions (Griffith et al., 2014). In ischemic muscles from VASP$^{-/-}$ mice, monocyte infiltration was significantly increased, and our data indicate that VASP deficiency elevates both CCL2 release by macrophages and the responsiveness of circulating monocytes and thereby synergistically increases leukocyte recruitment into the inflamed tissue. Assuming that the decrease in surface CCR2 expression reflects receptor internalization before desensitization and inactivation of signaling, our results suggest that VASP plays a role in the regulation of receptor trafficking.

Neutrophils express CCR2 at low levels compared with monocytes (Fujimura et al., 2015), but inflammatory stimuli increase neutrophil CCR2 levels, which is essential for neutrophil infiltration in inflammatory diseases (Souto et al., 2011; Talbot et al., 2015). Thus, we speculate that VASP-dependent CCR2 trafficking is also important for neutrophil infiltration into the inflamed hindlimb after ischemia. Consistently, CCR2 inhibition blocked both monocyte and neutrophil infiltration in the inflamed tissue of VASP$^{-/-}$ mice. Currently, however, we cannot rule out that VASP deficiency also affects the signaling of other chemokine receptors important for neutrophil or monocyte infiltration. A role for VASP in GPCR trafficking is so far unknown, but VASP was previously identified as a CXCR2-interacting protein (Neel et al., 2009). However, VASP knockdown in HL-60 cells with stable overexpression of CXCR2 was associated with impaired chemotaxis (Neel et al., 2009), and unlike with CCR2, we did not observe significant changes in CXCR2 surface expression between WT and VASP$^{-/-}$ cells.

VASP formed complexes with CCR2 and β-arrestin 2 in vesicle-like structures after leukocyte stimulation with CCL2, possibly reflecting receptor internalization. Such a phenomenon could well explain the apparent increase in CCL2-initiated signaling in VASP$^{-/-}$ leukocytes, and several known β-arrestin binding proteins that are involved in actin dynamics are also VASP-interacting proteins: zyxin, αII-spectrin, WASp, and components of the

Arp2/3 complex (Ball et al., 2000; Castellano et al., 2001; Skoble et al., 2001; Xiao et al., 2007, 2010; Benz et al., 2008a).

Consistent with the role of VASP in CCR2 trafficking, knockdown of Mena impaired clathrin-mediated endocytosis of the EGF receptor in HeLa cells, which explains the implication of Mena in EGF-dependent breast cancer invasion and metastasis (Philippar et al., 2008; Vehlow et al., 2013). However, there is also evidence that VASP is involved in receptor recycling, as VASP regulates the Rab11-dependent plasma membrane targeting of TGF-β receptors (Tu et al., 2015). How exactly VASP regulates these apparently opposing processes and which receptor classes and subclasses are affected, potentially in a cell type–specific manner, is currently unclear. Our results indicate that the underlying mechanism is independent of Rac1, which likely operates downstream of CCR2 receptor activation but may involve actin dynamics. In mammalian cells, the contribution of actin to progression and execution of endocytosis is still debated (Kaksonen et al., 2006; Mooren et al., 2012). Although our plain pharmacology approach suggests that actin dynamics may affect CCR2 receptor trafficking in monocytes, further experiments are required to analyze whether VASP-driven actin dynamics participate in the formation of membrane invaginations, fission of vesicles from the membrane, cytoplasmic vesicle movement, and/or recycling to the membrane. Currently, however, we cannot rule out that complex formation of VASP with CCR2 and β-arrestin may regulate CCR2 internalization in an actin-independent manner.

In addition to CCR2 receptor internalization, β-arrestin–VASP binding may be relevant for the regulation of inflammatory cytokine expression and activity. Indeed, β-arrestins inhibit TLR4 signaling and may have a direct role in regulating TLR sensitization/internalization, thereby suppressing inflammatory cytokine production (Jiang et al., 2013). Therefore, it is tempting to speculate that impaired β-arrestin 2 signaling alone or combined with reduced TLR4 internalization after LPS stimulation may contribute to the increased inflammatory cytokine expression in VASP$^{-/-}$ macrophages. Consistently, LPS-induced ERK1/2 phosphorylation, which requires β-arrestin 2 signaling, was significantly impaired in LPS- and IFNγ-treated VASP$^{-/-}$ macrophages.

Together, our data indicate that VASP is major regulator of leukocyte trafficking and polarization and suggest that transient VASP inhibition may be beneficial for the treatment of ischemic vascular diseases. However, it has to be considered that both in vivo models used in this study, hindlimb ischemia and thioglycollate-induced peritonitis, reflect sterile forms of inflammation. Given the role of VASP in macrophage phagocytosis (Coppolino et al., 2001; our own unpublished observations), further studies, such as cecal ligation and puncture, are required to investigate potential adverse effects of VASP inhibition, especially with regard to antibacterial host defense. However, at least two additional pathological conditions may be associated with detrimental aspects of VASP deletion in leukocytes: atherosclerosis and cancer. Both conditions are heavily associated with the recruitment and polarization of monocytes/macrophages, and it needs to be determined how VASP deletion would affect the progression of these diseases.

Materials and methods

Materials

DMEM-F12, RPMI 1640, FCS, nonessential amino acids, sodium pyruvate, MEM vitamins, penicillin/streptomycin, and cell culture–grade BSA were from Invitrogen; collagenase II from Worthington; and M-CSF, GM-CSF, IFNγ, IL-4, and CCL2 from Peprotech. Antibodies were as follows: anti–CD45-VioBlue (rat, 130-102-430) from Miltenyi Biotec; anti–Ly6G-APC-Cy7 (rat, 127624), CD11b A647 (rat, 101220), CD11b BV421 (rat, 101251), Ly6G PE (rat, 127607), anti–F4/80-PE-Cy7 (rat, 123114), anti–CD206-FITC (rat, 141704), anti–B220-FITC (rat, 103205) or -APC (rat, 103211), anti–CD192 (CCR2)-PE (rat, 150610), anti–CD11b BV605 (rat, 100742) from BioLegend; anti–Ly6C-PerCP-Cy5.5 (rat, 560525), anti–CD3-PE-CF594 (Armenian hamster, 562286), anti-CD31 (rat, 550274), anti–CD80-APC (Armenian hamster, 560016) from BD Bioscience; anti–CD31-PE-Cy7 (rat, 25-0311-82) from eBioscience; monoclonal and polyclonal anti-VASP antibodies (Benz et al., 2008b), anti–phospho-Tyr701-STAT (goat, SC-7988), anti-STAT6 (mouse, SC-374021), anti–phospho-Tyr641 STAT 6 (goat, SC-11762), monoclonal anti-VASP (mouse, SC-46668), monoclonal/polyclonal anti–β-arrestin 2 (mouse, SC-13140; goat, SC-6387) from Santa Cruz Biotechnology; anti-iNOS (rabbit, ALX-210-515) from Alexis; anti-CCR2 (goat, GTX45788) from Genetex; anti–STAT-1 (rabbit, 9172), anti–total ERK 1/2 (rabbit, 9102), anti–phospho-(Thr202/Tyr204, Thr185/Tyr187) Erk1/2 (rabbit, 4376) from Cell Signaling Technologies; anti–HA-tag (rabbit, ab6908) from Sigma-Aldrich; and anti–nonmuscle myosin (rabbit, ab75590) from Abcam. Peroxidase-conjugated antibodies were from Merck Millipore (anti–mouse, 401253; anti–rat, 401416; anti–rabbit, 401393; and anti–goat, 401515); Alexa Fluor–conjugated secondary antibodies were from Invitrogen (donkey anti–rabbit 488, A21206; donkey anti–goat 546, A11056; donkey anti–mouse 647, A31571; donkey anti–rat 594, A21209; and donkey anti–mouse 647, A31571). Plasmids encoding HA-tagged β-arrestin 2 and GST-β-arrestin 2 were gifts from R. Lefkowitz (Duke University, Durham, NC; Luttrell et al., 1999; Xiao et al., 2004); plasmids for mammalian and bacterial expression of His_6-tagged VASP were described previously (Benz et al., 2009). All other materials were obtained from Sigma-Aldrich or Applichem.

Animals

VASP$^{-/-}$ mice (Hauser et al., 1999) and their respective WT littermates were bred at the Goethe University Hospital animal facility. All animals were housed in conditions that conform to the Guide for the Care and Use of Laboratory Animals published by the US National Institutes of Health (publication 85-23). Both the University Animal Care Committee and the Federal Authority for Animal Research at the Regierungspräsidium Darmstadt (Hessen, Germany) approved the study protocol (#FU-1110). For the isolation of organs, mice were killed using 4% isoflurane in air and subsequent exsanguination or decapitation.

Hindlimb ischemia

Arteriogenic and angiogenic capacity was investigated in a mouse model of hindlimb ischemia as described previously (Abdel Malik et al., 2017). In brief, the deep femoral artery was ligated using an electric coagulator (Erbotom ICC50; Erbe), and the superficial

femoral artery and vein were completely excised. The overlying skin was closed with three surgical staples. Relative blood flow was determined by laser Doppler imaging (Laser Doppler Perfusion Imager System; Wilmington) at regular intervals for up to 21 d after surgery. The perfusion of the ischemic and nonischemic limb was calculated on the basis of colored histogram pixels. To minimize variables including ambient light and temperature and maintain a constant body temperature, mice were kept on a warming plate for 10 min before laser Doppler scans. Perfusion was expressed as the ratio of the ischemic to the nonischemic hindlimb.

Thioglycollate-induced peritonitis

Animals were injected with 3% thioglycollate medium to induce peritonitis. After 3 d, peritoneal fluid was collected, and leukocytes were suspended in 0.5% BSA-PBS for FACS staining. Samples were acquired with a LSRII/Fortessa flow cytometer (BD Biosciences) and analyzed using FlowJo software Vx (Treestar). Leukocytes were defined as neutrophils ($CD11b^+$, $Ly6G^+$), monocytes ($CD11b^+$, $Ly6G^-$, $Ly6C^{high}$), macrophages ($CD11b^+$, $Ly6G^-$, $Ly6C^{low}$, $F4/80^+$), M1-like macrophages ($CD80^{high}$, $CD206^{low}$), or M2-like macrophages ($CD80^{low}$, $CD206^{high}$).

CCR2 antagonist injection during peritonitis/hindlimb ischemia induction

The specific CCR2 inhibitor RS504393 (Sigma-Aldrich) was dissolved in DMSO to prepare a 10-mM stock solution. Before injection, the CCR2 stock solution was diluted in 0.9% NaCl containing 0.5% methylcellulose, 0.5% benzyl alcohol, and 0.1% Tween 20 (Kitagawa et al., 2004; Yang et al., 2010). The RS504393 suspension was injected daily i.p. at a final concentration of 4 mg/kg body weight per day, from 2 d before until 2 d after the induction of peritonitis/femoral artery excision.

µ-CT analyses

21 d after hindlimb ischemia induction, mice were killed and perfused with vasodilation buffer (DPBS; containing papaverine 4 mg/liter, adenosine 1 g/liter) followed by intravascular 1% PFA fixation. A mixture of 80% Neoprene latex (Neoprene Latex Dispersion 671 A; Dupont) and barium sulfate (3 g/ml; MicrOpaque oral solution; Guerbet) was used as contrast agent, and formic acid was used to polymerize the mixture. Mice were stored overnight in 4% PFA at 4°C and another two nights in 50% formic acid, then scanned in the micro-CT (Skyscan 1176; Bruker). Volumetric data were reconstructed with NRecon/InstaRecon CBR Server, premium software (Skyscan/InstaRecon). Image analysis, segmentation, and quantification were performed with Imalytics Preclinical software (Gremse-IT). The densities of the contrast medium and muscles were used as references. Quantification was expressed as total volume of ischemic/nonischemic hindlimb vessels.

BM transplantation

Groups of WT and VASP-KO mice were irradiated with two doses of 5 Gy using a BioBeam 2000 (Gamma-Service Medical). The next day, BM from femora and tibiae of WT and $VASP^{-/-}$ mice was collected, and mononuclear cells were isolated using Histopaque 1083 (Sigma-Aldrich). Four groups of mice were transplanted via caudal veins with BM mononuclear cells (2×10^6 cells/100 µl NaCl solution) as follows: WT BM transplanted into WT mice (WT-BM→WT), WT BM transplanted into $VASP^{-/-}$ mice (WT-BM→KO), $VASP^{-/-}$ BM transplanted into WT mice (KO-BM→WT), and $VASP^{-/-}$ BM transplanted into $VASP^{-/-}$ mice (KO-BM→KO). Treated mice were allowed to recover for 10 wk and subjected to hindlimb ischemia, followed by laser Doppler imaging measurements.

Macrophage differentiation and polarization

BM-derived leukocytes were cultured in basal RPMI medium (RPMI-1640 with nonessential amino acids, sodium pyruvate, MEM vitamins, and penicillin/streptomycin) supplemented with 10% FCS, 15 ng/ml M-CSF, and 15 ng/ml GM-CSF. After 7 d in culture, differentiated macrophages were polarized to proinflammatory M1 macrophages (10 ng/ml LPS and 1 ng/ml IFNγ for 6 or 24 h) or alternative M2 macrophage (25 ng/ml IL-4 for 24 or 48 h). For STAT1 inhibition studies, BM-derived macrophages were preincubated with 50 µM fludarabine (Selleckchem) for 1 h before M1 polarization. For STAT6 inhibition studies, BM-derived macrophages were preincubated with 2 µM AS1517499 (Axonmedchem) for 1 h before M2 polarization.

Cytometric bead array

Quantification of CXCL1 and CCL2 in cell culture supernatants and muscle lysates was performed by use of cytometric bead array flex sets (BD Biosciences). In brief, BM-derived macrophages from WT mice were polarized to M1 (10 ng/ml LPS + 1 ng/ml IFNγ) or M2 (25 ng/ml IL-4) or left untreated (control; CTL). 24 h later, the conditioned media were collected, and 25 µl of each sample was incubated with 25 µl CXCL1/CCL2-specific beads followed by CXCL1/CCL2-specific PE-labeled antibodies. After washing, samples were resuspended in 250 µl FACS Flow, measured on a LSRII/Fortessa flow cytometer, and evaluated with BD Bioscience FCAP software v.3.0.

Quantitative real-time PCR

After total RNA isolation (RNeasy; Qiagen), cDNA synthesis was performed with random hexamer primers (SuperScript III; Invitrogen). Reverse-transcription quantitative real-time PCR (RT-qPCR) was performed using SYBR Green Master Mix (Thermo Fisher Scientific) and appropriate primers in a MX3000 multiplex quantitative PCR system (Agilent Technologies). The relative RNA amounts were calculated using the $2^{-\Delta\Delta CT}$ method with 18S RNA as a reference. RT-qPCR primer sequences were as follows: 18S rRNA forward, 5′-CTTTGGTCGCTCGCTCCTC-3′, and reverse, 5′-CTGACCGGGTTGGTTTTGAT-3′; iNOS forward, 5′-GTGGTGACAAGCACATTTGG-3′, and reverse, 5′-GTTCGTCCC CTTCTCCTGTT-3′; IL-1β forward, 5′-CAGGCAGGCAGTATCACT CA-3′, and reverse, 5′-AGCTCATATGGGTCCGACAG-3′; YM-1 forward, 5′-CTGGAATTGGTGCCCCTACAA-3′, and reverse, 5′-CTG GTTGTCAGGGGAGTGTT-3′; IL-10 forward, 5′-CCAAGCCTTATC GGAAATGA-3′, and reverse, 5′-TTTTCACAGGGGAGAAATCG-3′; TNF-α forward, 5′-CCCGACTACGTGCTCCTCACC-3′, and reverse, 5′-CTCCAGCTGGAAGACTCCTCCCAG-3′; VEGF forward, 5′-GCA CTGGACCCTGGCTTTACTGCTGTA-3′, and reverse, 5′-GAACTT GATCACTTCATGGGACTTCTGCTC-3′; HIF1α forward, 5′-GAAATG

GCCCAGTGAGAAAA-3′, and reverse, 5′-CTTCCACGTTGCTGACTTGA-3′; HIF2α forward, 5′-CTAAGTGGCCTGTGGGTGAT-3′, and reverse, 5′-GTGTCTTGGAAGGCTTGCTC-3′; VASP QT01059828 QuantiTect Primer (Qiagen); Mm-CXCL1 QT00115647 QuantiTect Primer (Qiagen); Mm-CCL2 forward, 5′-GCTGTAGTTTTTGTCACCAAGC-3′, and reverse, 5′-GACCTTAGGGCAGATGCAGT-3′.

FACS isolation of BM-derived leukocytes

After 7-amino actinomycin D (eBioscience) exclusion to identify live cells, BM-derived leukocytes, isolated from WT (+/+) and VASP-KO (−/−) animals, were sorted into subsets of monocytes ($B220^-$, $CD3^-$, $CD11b^+$, $Ly6G^-$) and granulocytes ($B220^-$, $CD3^-$, $CD11b^+$, $Ly6G^+$) using FACS Aria III (BD Biosciences).

FACS analyses of leukocytes infiltration into ischemic muscles

After perfusion with PBS/heparin/vasodilation buffer, muscles from ischemic or control limbs were digested with collagenase II in DMEM-F12 medium (300 units/ml) at 37°C. Collected cells were suspended in 0.5% BSA-PBS, stained for flow cytometry with a LSRII/Fortessa flow cytometer (BD Biosciences), and analyzed using FlowJo software Vx (FlowJo). Myeloid cells were defined as $CD45^+$ and $CD11b^+$, with neutrophils ($Ly6G^+$), monocytes ($Ly6G^-$, $Ly6C^{high}$), macrophages ($Ly6G^-$, $Ly6C^{low}$, $F4/80^+$), M1-related macrophages ($CD80^{high}$, $CD206^{low}$), and M2-related macrophages ($CD80^{low}$, $CD206^{high}$).

RT-qPCR analyses of leukocyte infiltration into the hindlimb

After perfusion with PBS/heparin/vasodilation buffer, muscles from WT and $VASP^{-/-}$ limbs were digested with collagenase II in DMEM-F12 medium (300 units/ml) at 37°C. Collected cells were plated for 30 min onto tissue culture plates, extensively washed to enrich macrophage populations, and processed for RT-qPCR as outlined in Quantitative real-time PCR.

Transwell migration assay

Conditioned basal RPMI medium (750 µl) was collected from WT macrophages 24 h after M1 or M2 polarization or from nonpolarized controls and added to the lower compartment of Transwell filters (3.0-µm cell culture inserts from Greiner Bio-one). Optionally, 50 ng/ml CCL2 was used as chemoattractant in some assays. BM-derived leukocytes isolated from WT and VASP-KO (5×10^5 cells/350 µl basal RPMI medium containing 0.1% BSA) were added into the upper chamber of Transwell filters and allowed to migrate for 2 h toward the chemoattractant.

To investigate the impact of Rac1, cells were preincubated with 10 µM of the specific Rac1 inhibitor Ehop-016 (Montalvo-Ortiz et al., 2012) for 1 h before migration. Migrated leukocytes were collected and identified by FACS using a LSRII/Fortessa flow cytometer, and results were evaluated with FCAP software v.3.0 (BD Biosciences). Neutrophils were defined as $CD3^-$ $CD11b^+$ $Ly6G^{high}$ $Ly6C^{low}$ cells, and monocytes as $CD3^-$ $CD11b^+$ $Ly6G^{low}$, $Ly6C^{high}$ cells.

CCR2 chemokine receptor internalization

BM-derived leukocytes (10^6 cells) were stimulated with M1 conditioned medium for 5, 30, and 60 min; 50 ng/ml CCL2 for 5 min; or left untreated as control. To investigate the impact of Rac1 on CCR2 surface levels, BM-derived leukocytes were preincubated with 10 µM of the specific Rac1 inhibitor Ehop-016 (Montalvo-Ortiz et al., 2012) or 1 µg/ml of the Rac1 activator CN04 (Cytoskeleton) for 1 h before stimulation. To address the impact of actin dynamics on CCR2 surface levels, BM-derived leukocytes were preincubated without or with cytochalasin D (2.5, 10, or 15 µM), latrunculin A (0.5 µM), or latrunculin B (0.25, 0.5, or 5 µM) for 30 min before stimulation with M1 conditioned medium or 50 nM CCL2. Cells were collected by centrifugation at 2000 *g* for 1 min at 4°C and stained for FACS analysis. Mean fluorescence intensity of CCR2 in neutrophil and monocyte populations was measured by FACS using a LSRII/Fortessa flow cytometer. Neutrophils were defined as $CD11b^+$ $Ly6G^{high}$ $Ly6C^{int}$ cells, and monocytes as $CD11b^+$ $Ly6G^-$, $Ly6C^{high}$ cells.

Immunofluorescence microscopy

Hindlimbs

After perfusion with vasodilation buffer and zinc fixative solution, semimembranosus (thigh) and gastrocnemius (calf) muscles were fixed overnight at 4°C, embedded in TissueTek OCT Compound (Sakura), and immediately frozen on dry ice. Transverse cryosections (10 µm) were blocked/permeabilized with 5% goat serum (GeneTex) in PBS containing 0.2% Triton X-100 (PBS-T), followed by incubation with anti-CD31 antibodies overnight at 4°C. After extensive washing and exposure to Alexa Fluor secondary antibodies (2 h at room temperature), sections were washed, mounted with 50% glycerol in PBS containing 5% DABCO, and analyzed using a confocal microscope (SP8; Leica) equipped with a 40-fold oil-immersion objective. Images were acquired and prepared for presentation using LAS AF software (v.1.1.0.12420; Leica).

BM cells

BM was extracted from femora and tibiae of WT mice, washed in PBS, resuspended in basal RPMI medium, and seeded on poly-L-lysine (Biochrom)–coated µ-slides (Ibidi). Cells were stimulated with 150 nmol/liter CCL2 for 30 min, fixed with 4% formalin (Roth), washed with PBS, and incubated with mouse Fc Block (553142; BD Bioscience). After blocking/permeabilization with 5% normal donkey serum (GeneTex) in PBS-T, cells were incubated with diluted primary antibodies in the same solution, washed in PBS, incubated with Alexa Fluor 488/546/7647–conjugated secondary antibodies, washed again, and mounted with 50% glycerol in PBS containing 5% DABCO as an antifading agent. Cells were investigated at room temperature using a confocal laser scanning microscope (LSM 780; Zeiss) equipped with a 63-fold oil-immersion objective. Images were acquired, cropped, and prepared for presentation using ZEN software (v.2.1, black, 64 bit; Zeiss). Specificity of the stainings was confirmed by secondary-antibody-only controls that were imaged and processed with the same parameters as in the main figures. VASP-specific antibodies were validated with WT and $VASP^{-/-}$ leukocytes in immunofluorescent stainings and by FACS analyses.

Immunoprecipitations and GST pull-down assays

For immunoprecipitation, basal or M1 conditioned medium–stimulated mouse BM-derived leukocytes were lysed in buffer A: 40 mM Hepes-NaOH, pH 7.5, 100 mM NaCl, 1% Igepal CA-630,

and protease/phosphatase inhibitor cocktail. Lysates were clarified by centrifugation for 10 min at 20,000 *g* at 4°C and CCR2 or β-arrestin 2 were subjected to immunoprecipitation using either protein-specific antibodies or isotype control antibodies, followed by incubation with protein G–conjugated Sepharose beads (GE-Healthcare). After extensive washing with the lysis buffer, the precipitated material was analyzed by Western blotting using anti-VASP antibodies. For immunoprecipitations with tagged proteins, HEK cells were transfected with HA-tagged β-arrestin 2 (Luttrell et al., 1999) with or without His_6-tagged VASP (Benz et al., 2009) using Lipofectamine 2000 (Invitrogen). Cells were lysed and immunoprecipitated as detailed above, using anti-His_6-epitope tag affinity matrix (BioLegend), followed by Western blotting with anti-HA antibodies.

GST pull-down assays were performed as described (Benz et al., 2016). In brief, 500 ng purified His_6-VASP (Benz et al., 2009) was incubated with 5 µg GST-β-arrestin 2 (Xiao et al., 2004), equimolar amounts of GST alone (negative control), or GST-Spectrin-SH3 (positive control; Benz et al., 2013) coupled to glutathione Sepharose (GE-Healthcare) in buffer A supplemented with 25 ng/µl BSA to block unspecific interactions. After extensive washing, precipitated material was analyzed by Western blotting with anti-VASP antibodies.

Immunoblotting

Cells were lysed in TBS buffer (50 mM Tris-HCl and 150 mM NaCl, pH 7.4) containing 1% Triton X-100 and protease/phosphatase inhibitor cocktails. Lysates were clarified by centrifugation, and protein concentrations were measured by Bradford assay. 40 µg total protein was separated by standard 8–10% SDS-PAGE, blotted, and blocked in TBS supplemented with 3% BSA and 0.3% Tween-20. After overnight incubation with primary antibodies at 4°C, extensive washing, and incubation with peroxidase-conjugated secondary antibodies, proteins were visualized by enhanced chemiluminescence on a Fusion Solo imager (Vilber Lourmat).

Statistical analyses

Data are expressed as mean ± SEM. Statistical evaluation was performed using Student's *t* test for unpaired data, one-way ANOVA with Tukey posttest, or two-way ANOVA with Bonferroni posttest where appropriate. Values of $P < 0.05$ were considered statistically significant. Data distribution was assumed to be normal, but this was not formally tested.

Online supplemental material

Fig. S1 shows the gating strategy for flow cytometry analyses. Fig. S2 shows that VASP deletion increases M1 and M2 macrophage polarization in vitro. Fig. S3 shows expression levels of chemokines and chemokine receptors. Fig. S4 shows the impact of Rac1 and actin dynamics on CCR2 internalization. Fig. S5 shows that VASP deletion increases β-arrestin 2 protein levels; that CCR2 inhibition blocks the increased leukocyte infiltration into the peritoneal cavity of $VASP^{-/-}$ mice; and expression levels of early and late response genes after induction of M1 polarization. Video 1 shows collateral vessel formation in the thigh muscle of a WT mouse. Video 2 shows collateral vessel formation in the thigh muscle of a VASP-KO mouse.

Acknowledgments

The authors are indebted to Amparo Acker-Palmer, Rüdiger Popp, and Timo Frömel for conceptual input and to Isabel Winter, Mechtild Piepenbrock-Gyamfi, Katharina Engel-Herbig, and Praveen Mathoor for expert technical assistance (all Johann Wolfgang Goethe University, Frankfurt, Germany).

This work was supported by the Deutsche Forschungsgemeinschaft (SFB 834/A8 to P.M. Benz, SFB 834/A5 to I. Fleming, SFB 834/A2 to R.P. Brandes, SFB 834/Z1 to M.A. Rieger, SFB 1039/B6 to A. Weigert, and SFB 1039/B4 to B. Brüne). P.M. Benz was also supported by the German Center for Cardiovascular Research (DZHK B14-028 SE).

The authors declare no competing financial interests.

Author contributions: H. Laban and A. Weigert designed research, performed experiments, and analyzed data; J. Zink, A. Elgheznawy, C. Schürmann, L. Günther, R.A. Malik, S. Bothur, and S. Wingert performed experiments and analyzed data; R. Bremer generated the 3D videos; M.A. Rieger, B. Brüne, and R.P. Brandes helped to design and direct the project; I. Fleming designed research, helped to supervise the project, and wrote the manuscript; P.M. Benz conceived and planned the study, performed experiments, prepared the figures, and wrote the manuscript.

Submitted: 8 February 2017
Revised: 6 July 2017
Accepted: 26 January 2018

References

Abdel Malik, R., N. Zippel, T. Frömel, J. Heidler, S. Zukunft, B. Walzog, N. Ansari, F. Pampaloni, S. Wingert, M.A. Rieger, et al. 2017. AMP-activated protein kinase α2 in neutrophils regulates vascular repair via hypoxia-inducible factor-1α and a network of proteins affecting metabolism and apoptosis. *Circ. Res.* 120:99–109. https://doi.org/10.1161/CIRCRESAHA.116.309937

Anders, H.J., and L. Schaefer. 2014. Beyond tissue injury-damage-associated molecular patterns, toll-like receptors, and inflammasomes also drive regeneration and fibrosis. *J. Am. Soc. Nephrol.* 25:1387–1400. https://doi.org/10.1681/ASN.2014010117

Ball, L.J., R. Kühne, B. Hoffmann, A. Häfner, P. Schmieder, R. Volkmer-Engert, M. Hof, M. Wahl, J. Schneider-Mergener, U. Walter, et al. 2000. Dual epitope recognition by the VASP EVH1 domain modulates polyproline ligand specificity and binding affinity. *EMBO J.* 19:4903–4914. https://doi.org/10.1093/emboj/19.18.4903

Bear, J.E., and F.B. Gertler. 2009. Ena/VASP: Towards resolving a pointed controversy at the barbed end. *J. Cell Sci.* 122:1947–1953. https://doi.org/10.1242/jcs.038125

Bear, J.E., J.J. Loureiro, I. Libova, R. Fässler, J. Wehland, and F.B. Gertler. 2000. Negative regulation of fibroblast motility by Ena/VASP proteins. *Cell.* 101:717–728. https://doi.org/10.1016/S0092-8674(00)80884-3

Bennett, L.D., J.M. Fox, and N. Signoret. 2011. Mechanisms regulating chemokine receptor activity. *Immunology.* 134:246–256. https://doi.org/10.1111/j.1365-2567.2011.03485.x

Benz, P.M., C. Blume, J. Moebius, C. Oschatz, K. Schuh, A. Sickmann, U. Walter, S.M. Feller, and T. Renné. 2008a. Cytoskeleton assembly at endothelial cell–cell contacts is regulated by αII-spectrin–VASP complexes. *J. Cell Biol.* 180:205–219. https://doi.org/10.1083/jcb.200709181

Benz, P.M., S.M. Feller, A. Sickmann, U. Walter, and T. Renné. 2008b. Prostaglandin-induced VASP phosphorylation controls alpha II-spectrin breakdown in apoptotic cells. *Int. Immunopharmacol.* 8:319–324. https://doi.org/10.1016/j.intimp.2007.10.004

Benz, P.M., C. Blume, S. Seifert, S. Wilhelm, J. Waschke, K. Schuh, F. Gertler, T. Münzel, and T. Renné. 2009. Differential VASP phosphorylation controls remodeling of the actin cytoskeleton. *J. Cell Sci.* 122:3954–3965. https://doi.org/10.1242/jcs.044537

Benz, P.M., C.J. Merkel, K. Offner, M. Abeßer, M. Ullrich, T. Fischer, B. Bayer, H. Wagner, S. Gambaryan, J.A. Ursitti, et al. 2013. Mena/VASP and αII-spectrin complexes regulate cytoplasmic actin networks in cardiomyocytes and protect from conduction abnormalities and dilated cardiomyopathy. *Cell Commun. Signal.* 11:56. https://doi.org/10.1186/1478-811X-11-56

Benz, P.M., H. Laban, J. Zink, L. Günther, U. Walter, S. Gambaryan, and K. Dib. 2016. Vasodilator-stimulated phosphoprotein (VASP)-dependent and -independent pathways regulate thrombin-induced activation of Rap1b in platelets. *Cell Commun. Signal.* 14:21. https://doi.org/10.1186/s12964-016-0144-z

Castellano, F., C. Le Clainche, D. Patin, M.F. Carlier, and P. Chavrier. 2001. A WASp-VASP complex regulates actin polymerization at the plasma membrane. *EMBO J.* 20:5603–5614. https://doi.org/10.1093/emboj/20.20.5603

Chiba, Y., M. Todoroki, Y. Nishida, M. Tanabe, and M. Misawa. 2009. A novel STAT6 inhibitor AS1517499 ameliorates antigen-induced bronchial hypercontractility in mice. *Am. J. Respir. Cell Mol. Biol.* 41:516–524. https://doi.org/10.1165/rcmb.2008-0163OC

Coppolino, M.G., M. Krause, P. Hagendorff, D.A. Monner, W. Trimble, S. Grinstein, J. Wehland, and A.S. Sechi. 2001. Evidence for a molecular complex consisting of Fyb/SLAP, SLP-76, Nck, VASP and WASP that links the actin cytoskeleton to Fcgamma receptor signalling during phagocytosis. *J. Cell Sci.* 114:4307–4318.

Fan, H., L.M. Luttrell, G.E. Tempel, J.J. Senn, P.V. Halushka, and J.A. Cook. 2007. Beta-arrestins 1 and 2 differentially regulate LPS-induced signaling and pro-inflammatory gene expression. *Mol. Immunol.* 44:3092–3099. https://doi.org/10.1016/j.molimm.2007.02.009

Frank, D.A., S. Mahajan, and J. Ritz. 1999. Fludarabine-induced immunosuppression is associated with inhibition of STAT1 signaling. *Nat. Med.* 5:444–447. https://doi.org/10.1038/7445

Fujimura, N., B. Xu, J. Dalman, H. Deng, K. Aoyama, and R.L. Dalman. 2015. CCR2 inhibition sequesters multiple subsets of leukocytes in the bone marrow. *Sci. Rep.* 5:11664. https://doi.org/10.1038/srep11664

Fung, E., and A. Helisch. 2012. Macrophages in collateral arteriogenesis. *Front. Physiol.* 3:353. https://doi.org/10.3389/fphys.2012.00353

Griffith, J.W., C.L. Sokol, and A.D. Luster. 2014. Chemokines and chemokine receptors: Positioning cells for host defense and immunity. *Annu. Rev. Immunol.* 32:659–702. https://doi.org/10.1146/annurev-immunol-032713-120145

Han, Y.H., C.Y. Chung, D. Wessels, S. Stephens, M.A. Titus, D.R. Soll, and R.A. Firtel. 2002. Requirement of a vasodilator-stimulated phosphoprotein family member for cell adhesion, the formation of filopodia, and chemotaxis in dictyostelium. *J. Biol. Chem.* 277:49877–49887. https://doi.org/10.1074/jbc.M209107200

Hauser, W., K.P. Knobeloch, M. Eigenthaler, S. Gambaryan, V. Krenn, J. Geiger, M. Glazova, E. Rohde, I. Horak, U. Walter, and M. Zimmer. 1999. Megakaryocyte hyperplasia and enhanced agonist-induced platelet activation in vasodilator-stimulated phosphoprotein knockout mice. *Proc. Natl. Acad. Sci. USA.* 96:8120–8125. https://doi.org/10.1073/pnas.96.14.8120

Heil, M., T. Ziegelhoeffer, S. Wagner, B. Fernández, A. Helisch, S. Martin, S. Tribulova, W.A. Kuziel, G. Bachmann, and W. Schaper. 2004. Collateral artery growth (arteriogenesis) after experimental arterial occlusion is impaired in mice lacking CC-chemokine receptor-2. *Circ. Res.* 94:671–677. https://doi.org/10.1161/01.RES.0000122041.73808.B5

Jennissen, K., F. Siegel, M. Liebig-Gonglach, M.R. Hermann, S. Kipschull, S. van Dooren, W.S. Kunz, R. Fässler, and A. Pfeifer. 2012. A VASP-Rac-soluble guanylyl cyclase pathway controls cGMP production in adipocytes. *Sci. Signal.* 5:ra62. https://doi.org/10.1126/scisignal.2002867

Jiang, D., T. Xie, J. Liang, and P.W. Noble. 2013. β-Arrestins in the immune system. *Prog. Mol. Biol. Transl. Sci.* 118:359–393. https://doi.org/10.1016/B978-0-12-394440-5.00014-0

Kaksonen, M., C.P. Toret, and D.G. Drubin. 2006. Harnessing actin dynamics for clathrin-mediated endocytosis. *Nat. Rev. Mol. Cell Biol.* 7:404–414. https://doi.org/10.1038/nrm1940

Kitagawa, K., T. Wada, K. Furuichi, H. Hashimoto, Y. Ishiwata, M. Asano, M. Takeya, W.A. Kuziel, K. Matsushima, N. Mukaida, and H. Yokoyama. 2004. Blockade of CCR2 ameliorates progressive fibrosis in kidney. *Am. J. Pathol.* 165:237–246. https://doi.org/10.1016/S0002-9440(10)63292-0

Krause, M., and A. Gautreau. 2014. Steering cell migration: Lamellipodium dynamics and the regulation of directional persistence. *Nat. Rev. Mol. Cell Biol.* 15:577–590. https://doi.org/10.1038/nrm3861

Lee, W.J., S. Tateya, A.M. Cheng, N. Rizzo-DeLeon, N.F. Wang, P. Handa, C.L. Wilson, A.W. Clowes, I.R. Sweet, K. Bomsztyk, et al. 2015. M2 macrophage polarization mediates anti-inflammatory effects of endothelial nitric oxide signaling. *Diabetes.* 64:2836–2846. https://doi.org/10.2337/db14-1668

Limbourg, A., T. Korff, L.C. Napp, W. Schaper, H. Drexler, and F.P. Limbourg. 2009. Evaluation of postnatal arteriogenesis and angiogenesis in a mouse model of hind-limb ischemia. *Nat. Protoc.* 4:1737–1746. https://doi.org/10.1038/nprot.2009.185

Lin, W.H., S.E. Nelson, R.J. Hollingsworth, and C.Y. Chung. 2010. Functional roles of VASP phosphorylation in the regulation of chemotaxis and osmotic stress response. *Cytoskeleton (Hoboken).* 67:259–271.

Lu, G., R. Zhang, S. Geng, L. Peng, P. Jayaraman, C. Chen, F. Xu, J. Yang, Q. Li, H. Zheng, et al. 2015. Myeloid cell-derived inducible nitric oxide synthase suppresses M1 macrophage polarization. *Nat. Commun.* 6:6676. https://doi.org/10.1038/ncomms7676

Luttrell, L.M., S.S. Ferguson, Y. Daaka, W.E. Miller, S. Maudsley, G.J. Della Rocca, F. Lin, H. Kawakatsu, K. Owada, D.K. Luttrell, et al. 1999. Beta-arrestin-dependent formation of beta2 adrenergic receptor-Src protein kinase complexes. *Science.* 283:655–661. https://doi.org/10.1126/science.283.5402.655

Maghazachi, A.A. 2000. Intracellular signaling events at the leading edge of migrating cells. *Int. J. Biochem. Cell Biol.* 32:931–943. https://doi.org/10.1016/S1357-2725(00)00035-2

Moeller, M.J., A. Soofi, G.S. Braun, X. Li, C. Watzl, W. Kriz, and L.B. Holzman. 2004. Protocadherin FAT1 binds Ena/VASP proteins and is necessary for actin dynamics and cell polarization. *EMBO J.* 23:3769–3779. https://doi.org/10.1038/sj.emboj.7600380

Montalvo-Ortiz, B.L., L. Castillo-Pichardo, E. Hernández, T. Humphries-Bickley, A. De la Mota-Peynado, L.A. Cubano, C.P. Vlaar, and S. Dharmawardhane. 2012. Characterization of EHop-016, novel small molecule inhibitor of Rac GTPase. *J. Biol. Chem.* 287:13228–13238. https://doi.org/10.1074/jbc.M111.334524

Mooren, O.L., B.J. Galletta, and J.A. Cooper. 2012. Roles for actin assembly in endocytosis. *Annu. Rev. Biochem.* 81:661–686. https://doi.org/10.1146/annurev-biochem-060910-094416

Münzel, T., R. Feil, A. Mülsch, S.M. Lohmann, F. Hofmann, and U. Walter. 2003. Physiology and pathophysiology of vascular signaling controlled by guanosine 3′,5′-cyclic monophosphate-dependent protein kinase [corrected]. *Circulation.* 108:2172–2183. https://doi.org/10.1161/01.CIR.0000094403.78467.C3

Neel, N.F., M. Barzik, D. Raman, T. Sobolik-Delmaire, J. Sai, A.J. Ham, R.L. Mernaugh, F.B. Gertler, and A. Richmond. 2009. VASP is a CXCR2-interacting protein that regulates CXCR2-mediated polarization and chemotaxis. *J. Cell Sci.* 122:1882–1894. https://doi.org/10.1242/jcs.039057

Perri, S.R., B. Annabi, and J. Galipeau. 2007. Angiostatin inhibits monocyte/macrophage migration via disruption of actin cytoskeleton. *FASEB J.* 21:3928–3936. https://doi.org/10.1096/fj.07-8158com

Philippar, U., E.T. Roussos, M. Oser, H. Yamaguchi, H.D. Kim, S. Giampieri, Y. Wang, S. Goswami, J.B. Wyckoff, D.A. Lauffenburger, et al. 2008. A Mena invasion isoform potentiates EGF-induced carcinoma cell invasion and metastasis. *Dev. Cell.* 15:813–828. https://doi.org/10.1016/j.devcel.2008.09.003

Schlegel, N., and J. Waschke. 2009. VASP is involved in cAMP-mediated Rac 1 activation in microvascular endothelial cells. *Am. J. Physiol. Cell Physiol.* 296:C453–C462. https://doi.org/10.1152/ajpcell.00360.2008

Scholz, D., W. Ito, I. Fleming, E. Deindl, A. Sauer, M. Wiesnet, R. Busse, J. Schaper, and W. Schaper. 2000. Ultrastructure and molecular histology of rabbit hind-limb collateral artery growth (arteriogenesis). *Virchows Arch.* 436:257–270. https://doi.org/10.1007/s004280050039

Sechi, A.S., and J. Wehland. 2004. ENA/VASP proteins: Multifunctional regulators of actin cytoskeleton dynamics. *Front. Biosci.* 9:1294–1310. https://doi.org/10.2741/1324

Shireman, P.K. 2007. The chemokine system in arteriogenesis and hind limb ischemia. *J. Vasc. Surg.* 45:48–56.

Sica, A., and A. Mantovani. 2012. Macrophage plasticity and polarization: In vivo veritas. *J. Clin. Invest.* 122:787–795. https://doi.org/10.1172/JCI59643

Skoble, J., V. Auerbuch, E.D. Goley, M.D. Welch, and D.A. Portnoy. 2001. Pivotal role of VASP in Arp2/3 complex–mediated actin nucleation, actin branch-formation, and *Listeria monocytogenes* motility. *J. Cell Biol.* 155:89–100. https://doi.org/10.1083/jcb.200106061

Souto, F.O., J.C. Alves-Filho, W.M. Turato, M. Auxiliadora-Martins, A. Basile-Filho, and F.Q. Cunha. 2011. Essential role of CCR2 in neutrophil tissue infiltration and multiple organ dysfunction in sepsis. *Am. J. Respir. Crit. Care Med.* 183:234–242. https://doi.org/10.1164/rccm.201003-0416OC

Spiller, K.L., R.R. Anfang, K.J. Spiller, J. Ng, K.R. Nakazawa, J.W. Daulton, and G. Vunjak-Novakovic. 2014. The role of macrophage phenotype in vascularization of tissue engineering scaffolds. *Biomaterials*. 35:4477–4488. https://doi.org/10.1016/j.biomaterials.2014.02.012

Takeda, N., E.L. O'Dea, A. Doedens, J.W. Kim, A. Weidemann, C. Stockmann, M. Asagiri, M.C. Simon, A. Hoffmann, and R.S. Johnson. 2010. Differential activation and antagonistic function of HIF-alpha isoforms in macrophages are essential for NO homeostasis. *Genes Dev.* 24:491–501. https://doi.org/10.1101/gad.1881410

Talbot, J., F.J. Bianchini, D.C. Nascimento, R.D. Oliveira, F.O. Souto, L.G. Pinto, R.S. Peres, J.R. Silva, S.C. Almeida, P. Louzada-Junior, et al. 2015. CCR2 expression in neutrophils plays a critical role in their migration into the joints in rheumatoid arthritis. *Arthritis Rheumatol.* 67:1751–1759. https://doi.org/10.1002/art.39117

Trichet, L., C. Sykes, and J. Plastino. 2008. Relaxing the actin cytoskeleton for adhesion and movement with Ena/VASP. *J. Cell Biol.* 181:19–25. https://doi.org/10.1083/jcb.200710168

Tu, K., J. Li, V.K. Verma, C. Liu, D.D. Billadeau, G. Lamprecht, X. Xiang, L. Guo, R. Dhanasekaran, L.R. Roberts, et al. 2015. Vasodilator-stimulated phosphoprotein promotes activation of hepatic stellate cells by regulating Rab11-dependent plasma membrane targeting of transforming growth factor beta receptors. *Hepatology.* 61:361–374. https://doi.org/10.1002/hep.27251

Tucker, P.K., I.R. Evans, and W. Wood. 2011. Ena drives invasive macrophage migration in Drosophila embryos. *Dis. Model. Mech.* 4:126–134. https://doi.org/10.1242/dmm.005694

Tugal, D., X. Liao, and M.K. Jain. 2013. Transcriptional control of macrophage polarization. *Arterioscler. Thromb. Vasc. Biol.* 33:1135–1144. https://doi.org/10.1161/ATVBAHA.113.301453

Vehlow, A., D. Soong, G. Vizcay-Barrena, C. Bodo, A.L. Law, U. Perera, and M. Krause. 2013. Endophilin, Lamellipodin, and Mena cooperate to regulate F-actin-dependent EGF-receptor endocytosis. *EMBO J.* 32:2722–2734. https://doi.org/10.1038/emboj.2013.212

Wells, C.A., T. Ravasi, and D.A. Hume. 2005. Inflammation suppressor genes: Please switch out all the lights. *J. Leukoc. Biol.* 78:9–13. https://doi.org/10.1189/jlb.1204710

Xiao, K., S.K. Shenoy, K. Nobles, and R.J. Lefkowitz. 2004. Activation-dependent conformational changes in beta-arrestin 2. *J. Biol. Chem.* 279:55744–55753. https://doi.org/10.1074/jbc.M409785200

Xiao, K., D.B. McClatchy, A.K. Shukla, Y. Zhao, M. Chen, S.K. Shenoy, J.R. Yates III, and R.J. Lefkowitz. 2007. Functional specialization of beta-arrestin interactions revealed by proteomic analysis. *Proc. Natl. Acad. Sci. USA.* 104:12011–12016. https://doi.org/10.1073/pnas.0704849104

Xiao, K., J. Sun, J. Kim, S. Rajagopal, B. Zhai, J. Villén, W. Haas, J.J. Kovacs, A.K. Shukla, M.R. Hara, et al. 2010. Global phosphorylation analysis of beta-arrestin-mediated signaling downstream of a seven transmembrane receptor (7TMR). *Proc. Natl. Acad. Sci. USA.* 107:15299–15304. https://doi.org/10.1073/pnas.1008461107

Yang, D., L. Tong, D. Wang, Y. Wang, X. Wang, and C. Bai. 2010. Roles of CC chemokine receptors (CCRs) on lipopolysaccharide-induced acute lung injury. *Respir. Physiol. Neurobiol.* 170:253–259. https://doi.org/10.1016/j.resp.2010.02.002